IEEE Open Journal of Vehicular Technology

Received 31 January 2024; accepted 29 February 2024. Date of publication 5 March 2024;
date of current version 29 March 2024. The review of this article was coordinated by Editor Youngwook Ko.

Digital Object Identifier 10.1109/OJVT.2024.3373721

On the Performance of Interference-Based Energy-Harvesting-Enabled Wireless AF Relaying Communication Systems

YAZID M. KHATTABI [1,2] (Member, IEEE), YAZAN H. AL-BADARNEH [3] (Member, IEEE), AND MOHAMED-SLIM ALOUINI [4] (Fellow, IEEE)

[1]Department of Electrical Engineering, The University of Jordan, Amman 11942, Jordan
[2]College of Engineering and Technology, American University of the Middle East, Egaila 54200, Kuwait
[3]Department of Electrical Engineering, The University of Jordan, Amman 11942, Jordan
[4]Department of Computer, Electrical and Mathematical Sciences and Engineering, King Abdullah University of Science and Technology, Thuwal 23955, Saudi Arabia

CORRESPONDING AUTHOR: YAZID M. KHATTABI (e-mail: y.khattabi@ju.edu.jo).

ABSTRACT This article considers an interference-based radio-frequency energy harvesting (RF-EH)-empowered wireless dual-hop amplify-and-forward relaying system in which an ambient interferer is beneficially utilized as the solely free power source for EH and detrimentally considered as the dominant factor that corrupts its receivers. Three EH modes are considered and analyzed separately. In mode I, energy is harvested only by the source; in mode II, energy is harvested only by the relay; and in mode III, energy is harvested concurrently by both the source and relay. Under these modes, exact and approximate analytical expressions are derived for the system's outage probability, which are directly used to determine the system's delay-limited throughput as a performance figure of merit. Thorough numerical and simulation results are presented to verify the analytical work and to demonstrate the system's throughput performance under different system and channel parameters. For example, results reveal that for given channel conditions, increasing the interferer's power reduces the throughput in case of modes I and II, and has no effect on it in case of mode III. Also, for given interferer's power, improving the channel conditions between the interferer and a harvesting node, improves the throughput, while improving them between the interferer and a receiving node, degrades the throughput.

INDEX TERMS Energy harvesting, fading channels, interference, relaying systems, performance analysis.

I. INTRODUCTION

Employing green communication technologies has become an urgent need to enhance the self-sustainability and to prolong the lifetime of the ever-growing modern wireless networks. In general, attaining green communications is possible through several approaches including adopting energy-efficiency communication schemes, using extreme low-power consumption devices, and advocating wireless energy harvesting (EH) methods [1], [2], [3], [4], [5]. Among the diverse wireless EH methods, wireless radio frequency (RF) EH (RF-EH) has been shown as one of the most significant solutions toward green communications especially in large-scale and large-dense wireless Internet-of-Things (IoT) networks, and hence, it has gained noticeable interest in the research community [5], [6], [7]. In wireless RF-EH, propagating RF signals are utilized by energy constrained network devices that are equipped with dedicated EH circuits to harvest energy needed to support their own communication operations and/or to recharge their batteries [8]. Wireless RF-EH can be classified into three paradigms; namely, wireless power transfer (WPT), wireless-powered communication networks (WPCNs), and simultaneous wireless information and power transfer (SWIPT) [9]. In WPT, dedicated RF power transmitters are deployed to broadcast downlink non-informative RF signals to be utilized for energy harvesting by neighboring energy constrained users [10]. In WPCN, dedicated RF power transmitters are used with two active links, the downlink and the uplink. As similar as the WPT scheme, the downlink is

used by surrounding users only for energy harvesting purposes, while the uplink is used by the same users to traverse their own information signals through [11], [12]. In SWIPT, the downlink of classical centralized base stations is used to simultaneously carry information and energy to surrounding users equipped with energy harvesting and information decoding circuits [13], [14], [15]. The SWIPT paradigm is further categorized into three modes of operation; the time-splitting (TS) mode, the power-splitting (PS) mode, and the hybrid TS-PS mode [13], [16], [17], [18]. In the TS mode, the signaling period of the transmitted RF information signal is divided into two fractions; the first fraction is used for energy harvesting and the second one is used for information decoding. In the PS mode, and over the whole signaling period, the power of the RF information signal is divided at the receiving user into two fractions; the first fraction is used for energy harvesting and the remaining fraction is used for information decoding. In the hybrid TS − PS mode, the TS mode is employed as described above, but, over the second time fraction, the power is divided in accordance to the PS mode [18].

It should be noted that in the three aforementioned wireless RF-EH paradigms, dedicated and non-free power sources or centralized base stations are required. In this regard, and for the sake of improving green communication efficiency, the interest towards utilizing non dedicated and free RF power sources is currently increasing. Among such sources, ambient interferers, which are strongly inherited in wireless networks (especially in the modern ultra-dense 5G-based IoT ones [19]) have been recently suggested to be utilized as non-dedicated free power sources for RF-EH purposes [20]. In such interference-based RF-EH systems, energy constrained terminals can follow the TS-based harvest-then-transmit mode, in which the signaling period is divided into two fractions; one is allocated for RF-EH from the ambient interferer and the other is allocated to complete data transmission [21]. However, in real-world scenarios, implementing interference-based EH have practical challenges and limitations [20]. For example, despite that interference can be beneficially exploited for energy harvesting, it has the negative impact of corrupting received signals at system's receivers, which results in reducing system's reliability. Therefore, efficient and reliable interference mitigation and management techniques are recommended to be employed in such networks. Another key challenge is related to the fact that the amount of the harvested energy from interference signals is limited, which would not be enough to boost some critical communication operations. However, this limitation can be addressed by developing more energy-efficient beamforming algorithms to save energy at system's receivers. Further, the amount of the harvested energy from the interference is specified only by the interferer transmit power and the fading channel conditions between the interferer and the harvesting node, which are not guaranteed and not under control by any of the system's communicating devices (i.e., interferer is an unstable power source). Addressing this issue is also possible by developing adaptive EH algorithms that can switch to harvest energy from dedicated power sources when interferences signals are disappeared.

Because of its remarkable efficiency in reducing deep fading effects, augmenting network coverage, and increasing diversity gain and throughput, the technique of relaying has been considered among the emerging communication solutions that have paved the way to attain the growing demands on higher wireless access data rates [22], [23], [24], [25]. Thus, it has gained huge attraction in both researches and implementations and become among the core specifications in variant evolving technologies including 5G, IoT, device-to-device (D2D), vehicle-to-vehicle (V2V), non-orthogonal-multiple-access (NOMA), and unmanned aerial vehicle (UAV) networks and others [22], [23], [24], [26], [27], [28], [29], [30], [31], [32]. In relaying based wireless communication systems, a relaying node is dedicated to assist data traversal between two communicating nodes where two models are commonly used; dual-hop relaying (also called Type-I relaying) and dual-hop cooperative relaying (also called Type-II relaying) [33]. Dual-hop relaying is employed when the direct link between the two communicating nodes is blocked due to huge distance separation or deep fading where the relaying node is used to create alternative indirect communication link between the two blocked terminals. It has been shown that dual-hop relaying can significantly improve data throughput of receiving terminal [34]. Dual-hop cooperative relaying is used to create additional relay-aided indirect link to boost the already existing unblocked direct link between the two communicating nodes where both links are combined via certain diversity combining scheme. In accordance to the way of processing signals at the relaying node, relaying techniques are further classified as decode-and-forward (DF) and amplify-and-forward (AF) [35], [36], [37], [38]. With DF relaying, the relaying node decodes the received signal and then re-encodes it for transmission to the final receiving node. With AF relaying, the relaying node just re-transmits an amplified version of the received signal without any attempt of signal decoding. Hence, AF relaying offers less processing and implementation complexity and lower delay as compared to DF relaying, which makes it more attractive in the research community, see [39] and list of references therein. However, analytical performance investigation of AF-based relaying systems is more complicated as compared to that of DF relaying.

Communicating devices in wireless relaying systems no wonder need energy to support signal processing and forwarding, where the heavily depending on classical battery-based powering and recharging methods would be infeasible, especially, in large-dense and large-scale IoT and sensor networks. Thus, employing RF-EH harvesting approaches in wireless relaying systems is particularly important and has become an active area of research [18], [40], [41], [42], [43], [44], [45], [46], [47], [48], [49]. In [40], the authors have proposed the first RF-EH based dual-hop relaying communication system in which a source node is communicating with a destination node through an energy constrained AF relay that harvests

energy from the source information signal on the basis of the SWIPT protocol. Further, inspired by the TS and PS SWIPT protocols proposed for non relaying point-to-point systems, the authors have proposed two RF-EH protocols for their considered relaying system; namely the time switching-based relaying (TSR) and the power splitting-based relaying (PSR). In the TSR protocol, each signaling period is divided into three fractions; the first fraction is used by the relay to harvest energy from the source information signal, the second one is used by the relay to process the signal incoming from the source, and the remaining fraction is used to forward the relay's processed signal to the destination. In the PSR protocol, the first half of a signaling period is used for both EH and source to relay transmission and the second half is used for relay to destination transmission. During the first half, the received signal power is divided into two fractions, one for EH and one for source to relay transmission. The performance of the proposed system in [40] has been investigated by deriving approximate closed-form outage probability and approximate integral-form ergodic capacity expressions considering Rayleigh fading, which are also used to compute the system's delay-tolerant and delay-limited throughputs. Later in [18], [41], [42], [43], [44], [45], the RF-EH SWIPT based dual-hop relaying communication system proposed in [40] has been extended considering different system and channel assumptions. In [41], the authors have considered a dual-hop cooperative relaying system with DF energy constrained relay, where the system's outage probabilities for the TSR and PSR SWIPT RF-EH protocols have been derived in exact integral-form expressions considering Rayleigh fading. In [42], the authors have considered multiple DF energy constrained relays with best relay selection and hybrid TSR/PSR SWIPT RF-EH protocol, where the system's outage probability and ergodic capacity have been derived approximately based on the extreme value theorem in infinite series representation. In [43], the authors have considered a dual-hop cooperative relaying system with multiple energy constrained relays that harvest energy from the source information signal using the TSR SWIPT RF-EH protocol. The signal forwarded from the best relay is selected and combined with the direct-path signal via selection combining scheme. For both AF and DF relaying protocols, the system's outage probability has been derived in tight lower bound approximate expressions considering Nakagami-m fading. In [44], the authors have considered a dual-hop relaying communication system with energy constrained fixed-gain AF relay that harvests energy from the source information signal using the TSR SWIPT protocol subject to asymmetric Nakagami-m and $\alpha - \mu$ fading models. For such a system, the symbol error probability and the ergodic capacity have been derived in exact closed-form expressions in terms of the Fox's and the bivariate Fox's H-functions. In [45], the authors have considered a dual-hop cooperative relaying system with energy constrained AF relay that harvests energy from the source information signal using SWIPT protocols. For the TSR and the PSR protocols and considering Nakagmi-m fading, the authors have derived the exact expression for the system's bit error probability in terms of several special functions including the Meijer-G, the confluent hypergeometric and the Whittaker functions. In [18], the authors have considered a two users NOMA-based dual-hop cooperative relaying system with energy constrained DF relay that harvest energy from the source information signal using the hybrid TSR/PSR SWIPT protocol. The authors have derived exact closed-form outage probability expressions in terms of some special functions including the exponential integral function. It should be noted that in [40], [41], [42], [43], [44], [45], the energy constrained relay is assumed to harvest energy form the source information signal in accordance to the SWIPT protocol. In other words, the relay harvests non-free power from the source node, which is waste of allocated power resources. Thus, the interest towards proposing dual-hop relaying systems in which the relays harvest energy freely from ambient interferers has also gained attention [46], [47], [48], [49]. In [46], the authors have proposed a dual-hop relaying communication system in which the relay harvests energy from the source information signal (non-free energy) and from some ambient interferers (free energy) considering Rayleigh fading. They have also assumed that the interference signals corrupt the relay's received signal but not the destination's one. However, for the considered system, they have derived the outage probability and the delay-tolerant throughput in exact closed-form expressions. In [50], the authors have extended the EH based relaying system in [46] considering spectrum sharing environment. It should be noted that in [46] and [50] the authors have adopted the DF relaying protocol. In [47], the authors have reconsidered the model in [46] but with adopting the AF relaying protocol and with Nakagami-m fading. They have assumed that the relay generates the non-optimal variable amplification gain and the energy is harvested only by the relay while the source has its own power source. For such a system, the authors have derived the exact outage probability and the delay-tolerant throughput in double integral-form expressions. In [48], the authors have extended the work in [47] considering multiple AF relays with best relay selection scheme and Rayleigh fading, where the energy is also assumed to be harvested only by the relay. For this system, the authors have derived only upper bound expression for the outage probability and asymptotic expression for the throughput using the extreme value theorem. In [49], the authors have extended the work in [47] considering multi-hop relaying; however, they have derived the approximate outage probability using the upper bound SNR approach.

Although the previous works added significant insights, we can observe that most of them mainly focus on RF-EH based relaying systems in which only the relay is energy constrained and harvests whole or portion of its energy from the incoming source information signal. In this paper, and unlike previous literature works, we propose and study a Rayleigh fading RF-EH-enabled dual-hop AF relaying communication system in which some ambient interferer is considered as

the solely free source for energy harvesting.[1] As well, its detrimental effect on the system received signals at the relay and destination are taken into consideration. The AF relay is assumed to generate the optimal variable amplification gain. In addition, for sake of generic performance comparisons and gaining useful insights, we propose and separately investigate three energy harvesting modes. In mode I, it is assumed that only the source does not have constant power supply and needs to harvest energy from the ambient interferer. In mode II, it is assumed that only the relay does not have constant power supply and needs to harvest energy from the ambient interferer. In mode III, it is assumed that both the source and the relay do not have constant power supplies and need to harvest energy concurrently from the ambient interferer. In these three modes, we follow the TSR EH relaying scheme previously proposed in [40], i.e., each full signaling period is divided into three fractions, the first one is allocated for RF-EH (again, only from the interferer RF signal), the second one is for source-to-relay transmission, and the third one is for relay-to-destination transmission.

In particular and in this clause, we can summarize the contributions of this work as follows:

- The system end-to-end effective signal-to-interference-ratio (SIR) at the destination is first obtained for the three EH modes of interest.
- Starting from the obtained end-to-end SIRs, corresponding exact outage probability expressions are analytically derived in infinite-series representation for mode I and in integral-form for mode II and mode III.
- By lower-bound approximating the system end-to-end SIRs, tight lower-bound outage probability expressions are derived in closed-form for the three EH modes.
- The derived outage probability expressions are easy to compute via common computer softwares like MATALAB or MATHEMATICA, and they are given in terms of several significant system and channel parameters including the energy harvesting period, the energy conversion efficiency, the ambient interferer transmit power, the fading channel conditions of all system information and interference links.
- Correspondingly, the derived outage probability expressions are directly used to compute the system exact and upper-bound delay-limited throughput for the three EH modes and used as a figure of merit for performance investigation and comparisons.
- Comprehensive numerical and Monte-Carlo simulation results are provided to verify the analytical derivations and to gain insightful observations about the proposed system throughput performance subject to variant system and channel parameters.

The rest of the paper is organized as follow. Section II presents the system, channel, signaling, power generation and energy harvesting models for the proposed interference-based energy harvesting dual-hop relaying system. In Section III, the system outage probability is derived exactly and approximately for the different proposed energy harvesting modes. In Section IV, the system delay-limited throughput is determined. Numerical and Monte-Carlo simulation throughput results are presented in Section V. Finally, conclusions are drawn in Section VI.

[1]It is worthy noting that our proposed energy harvesting model is more energy efficient and offers less processing complexity as energy is harvested only from the ambient interferer and not from the source incoming information signal.

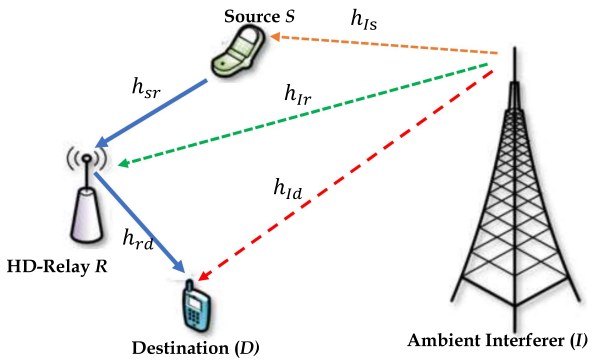

FIGURE 1. System model illustration.

II. SYSTEM MODEL

A. SYSTEM TOPOLOGY AND CHANNEL MODEL

As depicted in Fig. 1, we consider an AF dual-hop relaying communication system in which the source S is communicating with the destination D through a dedicated relaying terminal R under the effect of a single dominant ambient interferer I. The direct link between S and D is assumed to be absent due to the assumption of large distance separation or deep fading. Each of the system's operating terminals S, R, D and I is assumed to be equipped with single antenna and operates in the half-duplex mode. In Fig. 1, the dashed red lines refer to the interference channels from the interferer I to both S and D, the dashed green line refers to the interference channel from I to the R, and the solid blue lines refer to information channel links from S to R and from R to D. Whenever needed, the terminals S and R are assumed to be capable of harvesting energy from the broadcasted RF signal of the interferer I. Moreover, the broadcasted signal of I is assumed to corrupt the receiving portions of R and D as interfering signal.

All system wireless fading channels are assumed to be flat and quasi-static. It is also assumed that the channel state information (CSI) is perfectly known at the system receivers R and D.

The fading channel coefficients from S to R and from R to D are denoted by h_{sr} and h_{rd}, respectively, while those from I to S, R and D are denoted by h_{Is}, h_{Ir} and h_{Id}, respectively. All of the system fading channels are assumed to follow the Rayleigh distribution, i.e., h_{ab} is distributed as $\sim \mathcal{CN}(0, \lambda_{ab})$ and $|h_{ab}|^2$ is exponentially distributed ($\sim \exp(0, \lambda_{ab})$) with probability density function (PDF) of

$$f_{|h_{ab}|^2}(x) = \lambda_{ab} e^{-\lambda_{ab} x}, \quad x > 0, \tag{1}$$

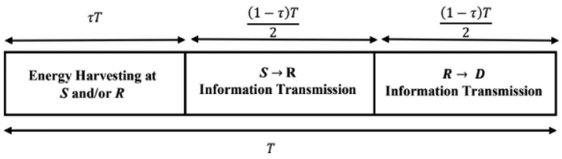

FIGURE 2. Time-frame structure for the proposed energy harvesting dual-hop relaying system with TSR protocol.

where $ab \in \{sr, rd, Is, Ir, Id\}$ and $\lambda_{ab}^{-1} = E[|h_{ab}|^2]$ accounts for the large-scale average fading power of the a-to-b link.

B. TSR EH PROTOCOL

As depicted in Fig. 2, a time period of T seconds in required to complete the transmission of one information block from S to D via R. According to the time-switching based EH protocol proposed in [40] for relaying systems, the time period T is divided into two fractions. A time fraction of τT seconds is used for EH either by S, R or both, where $0 \leqslant \tau < 1$.[2] The remaining time fraction $(1-\tau)T$ seconds is divided into two equal sub-fractions. The first sub-fraction $\frac{(1-\tau)}{2}T$ is allocated for S to R transmission. The remaining sub-fraction $\frac{(1-\tau)}{2}T$ is allocated for the R to D transmission. It is assumed that all energy harvested over the period τT is consumed, hence, S and R do not need batteries to store the energy they harvest.

C. POWER GENERATION

Let us first denote P_s^* for the transmit power of S and P_r^* for the transmit power of R.

1) POWER GENERATION AT SOURCE S

We consider two separate power generation methods that can be employed at S. In the first method, S can traditionally generate its own predetermined transmit power of P_s watts, i.e., no energy is harvested and $P_s^* = P_s$. In the second method, S is considered an energy constrained terminal and, over the time period τT seconds, can harvest energy from the ambient interferer I to generate its transmit power, where the amount of the harvested energy can be computed by

$$Eh_s = \zeta_s \tau T P_I |h_{Is}|^2, \tag{2}$$

where $0 < \zeta_s \leq 1$ is the energy conversion efficiency at S and P_I is the transmit power of the interferer I. The amount of harvested energy in (2) is then used to complete the information transmission from S to R over the time fraction $\frac{(1-\tau)}{2}T$ with transmit power of

$$P_s^* = \frac{Eh_s}{\frac{(1-\tau)}{2}T} = \frac{2\zeta_s \tau P_I |h_{Is}|^2}{(1-\tau)}. \tag{3}$$

[2]The case $\tau = 1$ is not considered because it implies no information transmission.

In summary, the transmit power of S can be given as

$$P_s^* = \begin{cases} P_s\,, & \text{(No energy harvesting at } S\text{)} \\ \frac{2\zeta_s \tau P_I |h_{Is}|^2}{(1-\tau)}\,, & \text{(Energy is harvested at } S \text{ from } I\text{).} \end{cases} \tag{4}$$

2) POWER GENERATION AT RELAY R

Similarly, we consider two separate power generation methods at R. In the first method, R generates its own predetermined transmit power of P_r watts, that is, no energy is harvested and $P_r^* = P_r$. In the second method, and over the EH time fraction τT, R harvests its energy from the ambient interferer I with amount of

$$Eh_r = \zeta_r \tau T P_I |h_{Ir}|^2, \tag{5}$$

where $0 < \zeta_r \leq 1$ refers to the energy conversion efficiency at R. Then, over the second time half $\frac{(1-\tau)}{2}T$, R uses this harvested energy to complete the information transmission from R to D with transmit power of

$$P_r^* = \frac{Eh_r}{\frac{(1-\tau)}{2}T} = \frac{2\zeta_r \tau P_I |h_{Ir}|^2}{(1-\tau)}. \tag{6}$$

In summary, the power generated at R can be given as

$$P_r^* = \begin{cases} P_r\,, & \text{(No energy harvesting at } R\text{)} \\ \frac{2\zeta_r \tau P_I |h_{Ir}|^2}{(1-\tau)}\,, & \text{(Energy is harvested at } R \text{ from } I\text{).} \end{cases} \tag{7}$$

D. PROPOSED EH MODES

In this paper, we separately consider three EH modes:

1) MODE I: ENERGY HARVESTING ONLY AT SOURCE S

In this mode, we assume that the source S is energy constrained device and can harvest its energy from the interferer I over the EH time period τT (i.e., $P_s^* = \frac{2\zeta_s \tau P_I |h_{Is}|^2}{(1-\tau)}$). On the other hand, the relay R is assumed to have its own power sources and can generate its own transmission power independently (i.e., $P_r^* = P_r$).

2) MODE II: ENERGY HARVESTING ONLY AT RELAY R

In this mode, we assume that the relay R is energy constrained device and can harvest its energy from the interferer I over the EH time period τT (i.e., $P_r^* = \frac{2\zeta_r \tau P_I |h_{Ir}|^2}{(1-\tau)}$), while the source S is assumed to have its own power sources and can generate its own transmission power independently (i.e., $P_s^* = P_s$).

3) MODE III: ENERGY HARVESTING AT BOTH S AND R

In this mode, we assume that both the source S and the relay R are energy constrained devices and can harvest their energy concurrently from the interferer I over the same EH time period τT (i.e., $P_s^* = \frac{2\zeta_s \tau P_I |h_{Is}|^2}{(1-\tau)}$ and $P_r^* = \frac{2\zeta_r \tau P_I |h_{Ir}|^2}{(1-\tau)}$).

E. SIGNALING MODEL AND END-TO-END SIR

The relaying link S-to-R-to-D accomplishes two transmission stages, which are described in the sequel. In the first stage, the

source S transmits its information signal, say x_s, to the relay R where the received signal is corrupted by both the AWGN noise and the interfering signal from the interferer I, that is

$$y_r = \sqrt{P_s^*} h_{sr} x_s + \sqrt{P_I} h_{Ir} x_I + n_r, \tag{8}$$

where P_s^* is given by (4) in accordance to the power generation method used at S, x_I is the interferer signal, and $n_r \sim \mathcal{CN}(0, N_o)$ is the AWGN noise sample with double-sided PSD of N_o. In the second transmission stage, the relay R employs the AF relaying scheme and amplifies y_r in (8) by amplification gain G. For sake of restricting the relay's transmit power by P_r^* and under the assumption that the interference power dominates the noise power (i.e., $\frac{N_o}{P_I} \to 0$ [21], [49], [51]), the gain G is produced as

$$G = \sqrt{\frac{1}{P_s^* |h_{sr}|^2 + P_I |h_{Ir}|^2}}. \tag{9}$$

Then, the relay R forwards the amplified signal Gy_r to the final destination D where the received signal is also affected by the AWGN noise and the interfering signal from I, hence, D receives the signal

$$y_d = \sqrt{P_r^*} h_{rd} G y_r + \sqrt{P_I} h_{Id} x_I + n_d, \tag{10}$$

where $n_d \sim \mathcal{CN}(0, N_o)$ is the AWGN noise sample. Considering (8) in (10) gives y_d as

$$\begin{aligned} y_d = {} & \sqrt{P_s^*}\sqrt{P_r^*} h_{sr} h_{rd} G x_s + \sqrt{P_I}\sqrt{P_r^*} h_{Ir} h_{rd} G x_I \\ & + \sqrt{P_r^*} h_{rd} G n_r + \sqrt{P_I} h_{Id} x_I + n_d. \end{aligned} \tag{11}$$

Now, under the above assumption that $\frac{N_o}{P_I} \to 0$, the end-to-end SIR at the destination D can be obtained from (11) as

$$\mathcal{X} = \frac{P_s^* P_r^* G^2 |h_{sr}|^2 |h_{rd}|^2}{P_I P_r^* |h_{Ir}|^2 |h_{rd}|^2 G^2 + P_I |h_{Id}|^2}. \tag{12}$$

Substituting (9) into (12) along with doing some simplifications gives $\mathcal{X}$ as

$$\mathcal{X} = \frac{P_s^* P_r^* |h_{sr}|^2 |h_{rd}|^2}{P_I P_r^* |h_{Ir}|^2 |h_{rd}|^2 + P_I P_s^* |h_{sr}|^2 |h_{Id}|^2 + P_I^2 |h_{Ir}|^2 |h_{Id}|^2}. \tag{13}$$

In the following section, the system outage probability is analyzed.

III. OUTAGE PROBABILITY ANALYSIS

Assuming a fixed source transmission rate of R bits/sec/Hz, the outage probability can be evaluated by

$$P_{\text{out}} = \mathrm{P}_r \{\mathcal{X} < \gamma_{\text{th}}\}, \tag{14}$$

where $\mathcal{X}$ is the end-to-end SIR in (13) and $\gamma_{\text{th}} = 2^R - 1$ is the threshold SIR value for correct data detection at the destination D. In the sequel, we use (13) and (14) to derive the system outage probability for the three EH modes of interest.

A. MODE I: ENERGY HARVESTING ONLY AT SOURCE S

1) EXACT OUTAGE PROBABILITY

Theorem 3.1: The exact outage probability of the considered interference-based dual-hop AF relaying system with energy harvesting mode I in which energy is harvested only at S can be computed by

$$\begin{aligned} P_{\text{out}}^{\text{I}} = {} & \frac{\lambda_{Is} \gamma_{\text{th}} (1-\tau) \lambda_{sr}}{2\zeta_s \tau \lambda_{Ir}} e^{-\left(\frac{(1-\tau)\lambda_{sr}\lambda_{Is}\gamma_{\text{th}}}{2\zeta_s \tau \lambda_{Ir}}\right)} \\ & \times \text{Ei}\left(\frac{(1-\tau)\lambda_{sr}\lambda_{Is}\gamma_{\text{th}}}{2\zeta_s \tau \lambda_{Ir}}\right) + \frac{\lambda_{Is}\gamma_{\text{th}}^2(\gamma_{\text{th}}+1)}{\left(\gamma_{\text{th}} + \frac{P_r \lambda_{Id}}{P_I \lambda_{rd}}\right)^2} \\ & \times \sum_{n=0}^{\infty} \left[\beta_n \sum_{k=0}^{n} \binom{n}{k} \upsilon_{k,n} \right. \\ & \left. \times \Psi\left(k+2, 1+k-n; \frac{(1-\tau)\lambda_{sr}\lambda_{Is}\gamma_{\text{th}}}{2\zeta_s \tau \lambda_{Ir}}\right) \right], \end{aligned} \tag{15}$$

where

$$\beta_n = \frac{(2)_n \left((2)_n + (1)_n (1+\gamma_{\text{th}})\right)}{2(3)_n n!}$$

$$\upsilon_{k,n} = \left(\frac{2\zeta_s \tau \lambda_{Ir}}{(1-\tau)\lambda_{sr}}\right)^{k-n-1} \left(\gamma_{\text{th}} - \frac{\gamma_{\text{th}}(\gamma_{\text{th}}+1)}{\gamma_{\text{th}} + \frac{P_r \lambda_{Id}}{P_I \lambda_{rd}}}\right)^{n-k} \times \Gamma(k+2) \left(\frac{(1-\tau)\lambda_{sr}\gamma_{\text{th}}}{2\zeta_s \tau \lambda_{Ir}}\right)^{k-n},$$

where $\gamma_{\text{th}} = 2^R - 1$ with R is the transmission data rate, $\text{Ei}(x) = -\int_{-x}^{\infty} \frac{e^{-t}}{t} dt$ refers to the exponential integral function [52, 8.211], $\Psi(\cdot,\cdot;\cdot)$ is the Tricomi hypergeometric function [52, Eq. (9.211–4.8)], $(a)_n = \frac{\Gamma(a+n)}{\Gamma(a)}$ denotes for the Pochhammer symbol, $(\cdot)!$ is the factorial operator, and $\Gamma(\cdot)$ is the gamma function.

Proof: See Appendix A. ■

2) APPROXIMATE OUTAGE PROBABILITY

Theorem 3.2: The outage probability of the considered interference-based dual-hop AF relaying system with energy harvesting mode I in which energy is harvested only at S can be computed using the following tight lower-bound closed-from expression.

$$\begin{aligned} P_{\text{out,Low}}^{\text{I}} = {} & 1 - \left[\frac{P_r \lambda_{Id}}{P_I \lambda_{rd} \gamma_{\text{th}} + P_r \lambda_{Id}}\right] \frac{\gamma_{\text{th}}(1-\tau)\lambda_{Is}\lambda_{sr}}{2\zeta_s \tau \lambda_{Ir}} \\ & \times \Psi\left(2, 2; \frac{\gamma_{\text{th}}(1-\tau)\lambda_{Is}\lambda_{sr}}{2\zeta_s \tau \lambda_{Ir}}\right). \end{aligned} \tag{16}$$

Proof: See Appendix B. ■

B. MODE II: ENERGY HARVESTING ONLY AT RELAY R

1) EXACT OUTAGE PROBABILITY

Theorem 3.3: The exact outage probability of the considered interference-based dual-hop AF relaying system with energy

harvesting mode II in which energy is harvested only at R can be computed by

$$P_{\text{out}}^{\text{II}} = \frac{\gamma_{\text{th}}}{\gamma_{\text{th}}+\beta_s} - \int_0^{\infty} \frac{\beta_s \alpha_r}{(z+\gamma_{\text{th}}+\beta_s)^2} \frac{(z+\gamma_{\text{th}}+1)\gamma_{\text{th}}}{z} \times e^{\left(\alpha_r \frac{(z+\gamma_{\text{th}}+1)\gamma_{\text{th}}}{z}\right)} \text{Ei}\left(-\alpha_r \frac{(z+\gamma_{\text{th}}+1)\gamma_{\text{th}}}{z}\right) \text{d}z, \tag{17}$$

where

$$\beta_s = \frac{\lambda_{Ir} P_s}{\lambda_{sr} P_I}$$
$$\alpha_r = \frac{(1-\tau)\lambda_{rd}\lambda_{Ir}}{2\zeta_r \tau \lambda_{Id}}. \tag{18}$$

Proof: See Appendix C. ■

2) APPROXIMATE OUTAGE PROBABILITY

Theorem 3.4: The outage probability of the considered interference-based dual-hop AF relaying system with energy harvesting mode II in which energy is harvested only at R can be computed using the following tight lower-bound closed-from expression.

$$P_{\text{out,Low}}^{\text{II}} = 1 - \lambda_{Ir}\Gamma(2)\frac{\lambda_{rd}\gamma_{\text{th}}}{\lambda_{Id}}\frac{1-\tau}{2\zeta_r\tau} \times \Psi\left(2,2;\frac{\lambda_{rd}\gamma_{\text{th}}}{\lambda_{Id}}\frac{1-\tau}{2\zeta_r\tau}\left(\lambda_{Ir}+\frac{P_I\lambda_{sr}\gamma_{\text{th}}}{P_s}\right)\right). \tag{19}$$

Proof: See Appendix D. ■

C. MODE III: ENERGY HARVESTING AT BOTH SOURCE AND RELAY

1) EXACT OUTAGE PROBABILITY

Theorem 3.5: The exact outage probability of the considered interference-based dual-hop AF relaying system with energy harvesting mode III in which energy is harvested at both S and R can be computed by

$$P_{\text{out}}^{\text{III}} = 1 - \int_0^{\infty} \alpha_r \frac{(z+\gamma_{\text{th}}+1)\gamma_{\text{th}}}{z} e^{-\left(\alpha_r \frac{(z+\gamma_{\text{th}}+1)\gamma_{\text{th}}}{z}\right)} \times \text{Ei}\left(-\alpha_r \frac{(z+\gamma_{\text{th}}+1)\gamma_{\text{th}}}{z}\right) \alpha_s \Psi\left(2,1;\alpha_s(z+\gamma_{\text{th}})\right) \text{d}z, \tag{20}$$

where

$$\alpha_r = \frac{(1-\tau)\lambda_{rd}\lambda_{Ir}}{2\zeta_r\tau\lambda_{Id}}$$
$$\alpha_s = \frac{(1-\tau)\lambda_{Is}\lambda_{sr}}{2\zeta_s\tau\lambda_{Ir}}. \tag{21}$$

Proof: See Appendix E. ■

2) APPROXIMATE OUTAGE PROBABILITY

Theorem 3.6: The outage probability of the considered interference-based dual-hop AF relaying system with energy harvesting mode III in which energy is harvested at both S and R can be computed using the following tight lower-bound closed-from expression

$$P_{\text{out,Low}}^{\text{III}} = 1 - \lambda_{Is}\frac{\Gamma(2)\lambda_{rd}(1-\tau)^3\gamma_{\text{th}}^2}{8\zeta_r\zeta_s\tau^3\lambda_{Id}} \sum_{k=0}^{n} \frac{(-1)^k (2)_k (1)_k}{k!} \times \left(\frac{4\zeta_s\zeta_r\tau^2\lambda_{Id}\Gamma(k+3)}{\lambda_{rd}(1-\tau)^2\gamma_{\text{th}}}\right)^{k+2} \times \Psi\left(k+3,2;\frac{\lambda_{Is}\lambda_{sr}\gamma_{\text{th}}(1-\tau)}{\lambda_{Ir}2\zeta_s\tau}\right). \tag{22}$$

Proof: See Appendix F. ■

IV. DELAY-LIMITED THROUGHPUT

In the delay-limited transmission scheme, the outage probability is the essential quantity to compute the delay-limited throughput. Provided that the source is communicating R bits/sec/Hz and, as deposited in Fig. 2, $(1-\tau)T/2$ is the effective end-to-end communication time from the source S to the destination D in the block of T seconds, the delay-limited throughput at the destination can be computed as [40]

$$\mathcal{R}_{DL}(\tau) = (1-P_{\text{out}})R\frac{(1-\tau)T/2}{T} = (1-P_{\text{out}})R\frac{(1-\tau)}{2}, \tag{23}$$

where P_{out} is given exactly and approximately in the previous section for the three EH modes under study. Notice that computing (23) using the lower-bound outage probabilities results in upper-bound delay-limited throughput.

It is worth pointing out that the throughput-optimal energy harvesting time, denoted by τ^*, can be obtained according to the following problem

$$\tau^* = \arg\max_{\tau} \mathcal{R}_{DL}(\tau)$$
$$\text{s.t. } 0 < \tau < 1. \tag{24}$$

Correspondingly, the optimal throughput is $\mathcal{R}_{DL}(\tau^*)$. Unfortunately, utilizing the analytical expressions for $\mathcal{R}_{DL}(\tau)$ derived for the three modes will not lead to closed-form solution for τ^*. Hence, we resort to numerical solution where τ^* can be efficiently computed using exhaustive search.

V. NUMERICAL AND SIMULATION RESULTS

In this section, we numerically investigate the delay-limited throughput of all Modes for different system parameters. The correctness of obtained analytical results is validated using extensive Monte Carlo simulations, where the throughput is being evaluated by averaging one million independent realizations. For simplicity but without loss of generality, the throughput evaluation considers the following default values: $\lambda_{sr} = \lambda_{rd} = 1$, and $\zeta_r = \zeta_s = 1$. For the simulation setup under consideration, we find that the infinite series in the

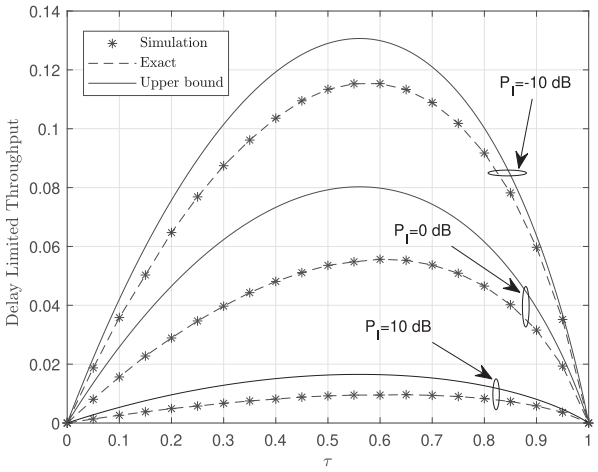

FIGURE 3. Delay limited throughput of mode *I* versus the energy harvesting time τ for different values of P_I at $\lambda_{Is} = 4$, $\lambda_{sr} = 1$, $\lambda_{rd} = 1$, $\lambda_{Ir} = 3$, and $\lambda_{Id} = 4$.

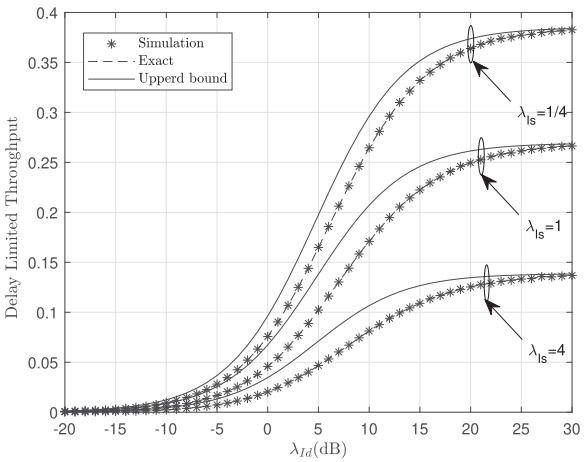

FIGURE 4. Delay limited throughput of mode *I* versus λ_{Id} for different values of λ_{Is} at $P_I = 1$, $\lambda_{sr} = 1$, $\lambda_{rd} = 1$, and $\lambda_{Ir} = 3$.

exact outage probability expression in (15) is truncated with accuracy using the first 74 terms, which confirms its quick convergence. The integrals in Theorems 3.3 and 3.5 do not admit analytical solutions, hence, we resort to numerical integration for evaluating the exact outage performance.

In Fig. 3, the delay-limited throughput of Mode I is depicted against τ for different values of P_I. We first note that the exact throughput accurately matches with the Monte-Carlo simulations. We also observe that the upper bound is reasonably tight for all $0 < \tau < 1$. It can be also seen that the throughput improves as P_I decreases. This can be justified as follows: although the source can harvest more energy when P_I increases, higher values of P_I will result in higher interference power at the relay and destination, which inevitably leads to worse throughput performance. Furthermore, we can observe that increasing τ, increases the throughput starting from zero up to its maximum value at some specific τ value. Then, over this specific value of τ, the throughput starts decreasing back to zero. This is due to the fact that for small values of τ, there is less time allocated for energy harvesting, which means less harvested energy (or less transmit power), and thus, less throughput attained at the final destination. On the other hand, for large values of τ, more time is consumed on energy harvesting and less time is allocated for actual information transmission, which also reduces the throughput at the destination node. More results on optimal delay-limited throughput are presented in Fig. 13.

Fig. 4, illustrates delay-limited throughput of Mode I against λ_{Id} for different values of λ_{Is}. We note that the exact throughput matches perfectly with the Monte Carlo simulations. It is evident from this figure that the throughput improves as λ_{Id} increases. This is expected, since larger values of λ_{Id} imply less interference power at the destination. Nevertheless, we can observe that after some higher λ_{Id} value (for e.g. 20 dB), the throughput enhancement with it becomes slow. We also observe that the throughput improves as the

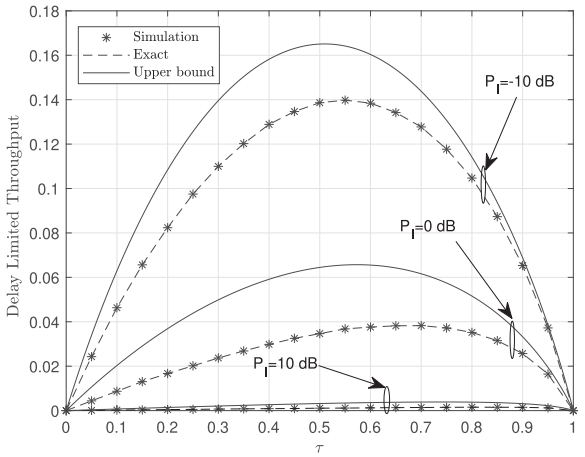

FIGURE 5. Delay limited throughput of mode *II* versus the energy harvesting time τ for different values of P_I at $\lambda_{sr} = 1$, $\lambda_{rd} = 1$, $\lambda_{Ir} = 3$, and $\lambda_{Id} = 4$.

λ_{Is} decreases. This is because smaller values of λ_{Is} will lead to better channel conditions between the interferer and the source, which results in higher harvested energy at the source.

In Fig. 5, the delay-limited throughput of Mode II is plotted against τ for different values of P_I. We confirm the correctness of the exact throughput using Monte-Carlo simulations. It can be seen from the figure that the throughput improves as P_I decreases and the upper bound is reasonably tight for all $0 < \tau < 1$.

Fig. 6, illustrates delay-limited throughput of Mode II against λ_{Id} for different values of λ_{Ir}. As expected, the throughput improves as λ_{Id} grows large. In addition, the throughput improves as λ_{Ir} decreases. This is due to the fact that smaller values of λ_{Ir} will result in better channel conditions between the interferer and the relay, which leads to larger harvested energy at the relay.

Figs. 7 and 8 depict the delay-limited throughput of Mode III against τ for different values of λ_{Is} and λ_{Id}, respectively.

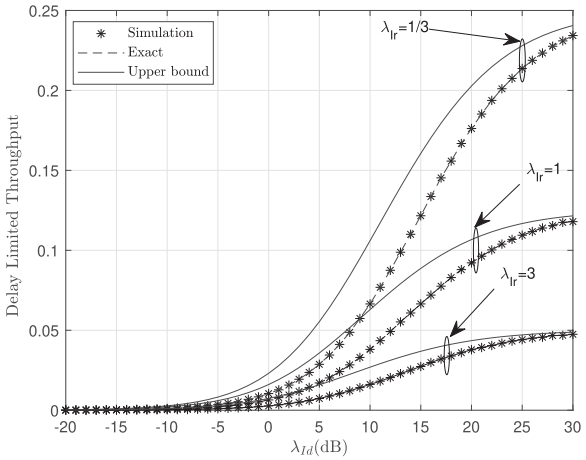

FIGURE 6. Delay limited throughput of mode *II* versus λ_{Id} for different values of λ_{Ir} at $P_I = P_S = 1$, $\lambda_{sr} = 1$, and $\lambda_{rd} = 1$.

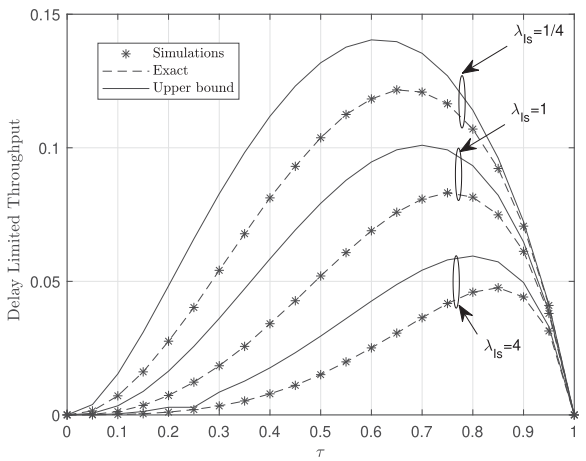

FIGURE 7. Delay limited throughput of mode *III* versus the energy harvesting time τ for different values of λ_{Is} at $\lambda_{sr} = 1$, $\lambda_{rd} = 1$, $\lambda_{Ir} = 3$, and $\lambda_{Id} = 4$.

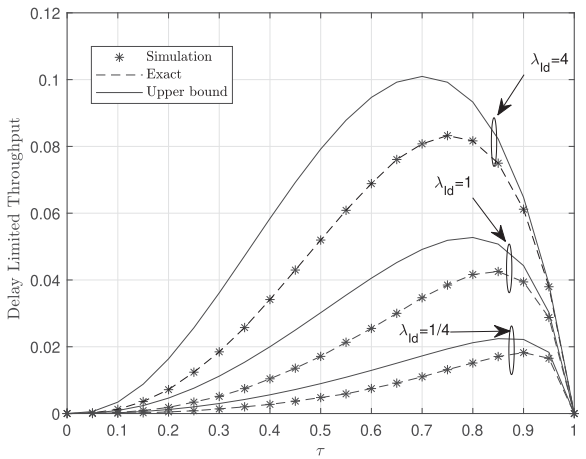

FIGURE 8. Delay limited throughput of mode *III* versus the energy harvesting time τ for different values of λ_{Id} at $\lambda_{sr} = 1$, $\lambda_{rd} = 1$, $\lambda_{Ir} = 3$, and $\lambda_{Is} = 1$.

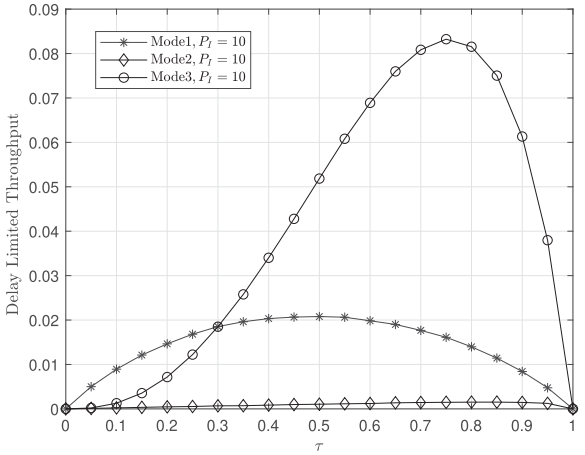

FIGURE 9. Delay limited throughput of all modes versus the energy harvesting time τ at $P_I = 10$, $\lambda_{sr} = 1$, $\lambda_{rd} = 1$, $\lambda_{Ir} = 3$, $\lambda_{Id} = 4$, and $\lambda_{Is} = 1$.

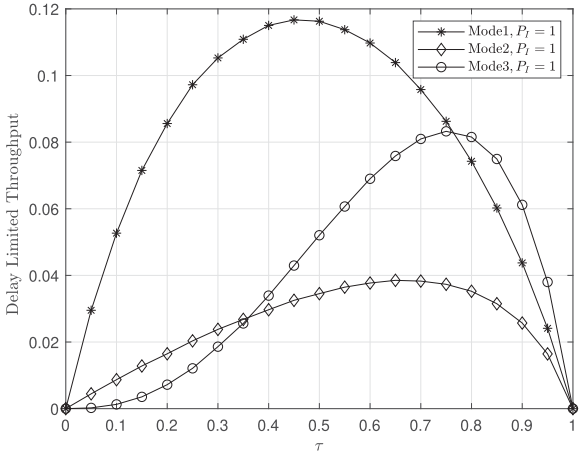

FIGURE 10. Delay limited throughput of all modes versus the energy harvesting time τ at $P_I = 1$, $\lambda_{sr} = 1$, $\lambda_{rd} = 1$, $\lambda_{Ir} = 3$, $\lambda_{Id} = 4$, and $\lambda_{Is} = 1$.

It is evident from Fig. 7 that larger values of λ_{Is} will result in throughput degradation since the source will harvest less energy as λ_{Is} increases. It can be also shown from Fig. 8 that the throughput improves as λ_{Id} increases, as expected.

In Figs. 9, 10 and 11, we study the throughput of all modes against τ when $P_I = 10$, $P_I = 1$, and $P_I = 0.1$, respectively. It can be observed from Fig. 9 that when P_I is large (i.e., $P_I = 10$), mode III is the best in terms of throughput for $\tau > 0.3$. This is an evident that Mode III is of more practical interest at larger values of P_I. This is due to the fact that when the energy harvesting is employed at either only the source (Mode I) or the relay (Mode II), higher values of P_I causes higher interference power at the destination, which leads to throughput degradation.

In Fig. 10, we observe that Mode I achieves the best throughput performance when $P_I = 1$ for $\tau < 0.75$ and Mode III achieves the best throughput for $\tau > 0.75$. We also observe that Mode III achieves much better than Mode II for $\tau > 0.35$. Accordingly, it can be concluded that Mode I and Mode III

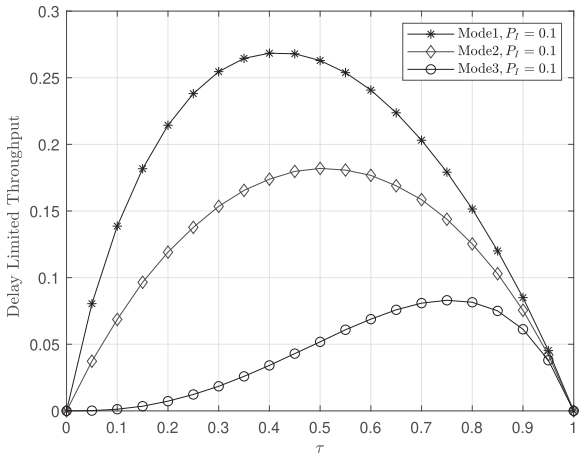

FIGURE 11. Delay limited throughput of all modes versus the energy harvesting time τ at $P_I = 0.1$, $\lambda_{sr} = 1$, $\lambda_{rd} = 1$, $\lambda_{Ir} = 3$, $\lambda_{Id} = 4$, and $\lambda_{Is} = 1$.

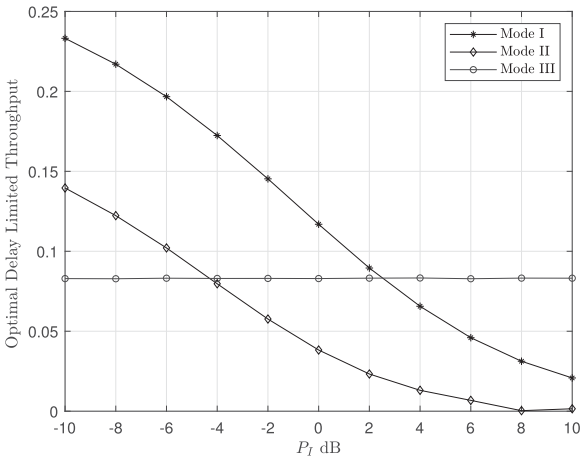

FIGURE 13. Optimal delay-limited throughput of all Modes versus P_I, $\lambda_{sr} = 1$, $\lambda_{rd} = 1$, $\lambda_{Ir} = 3$, $\lambda_{Id} = 4$, and $\lambda_{Is} = 1$.

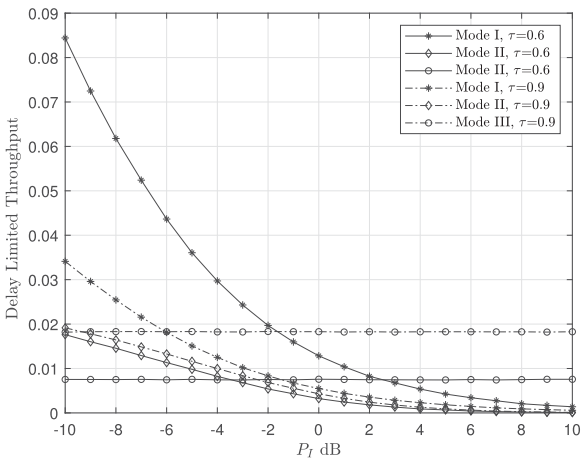

FIGURE 12. Delay limited throughput of all modes versus interferer transmit power for energy harvesting time $\tau = 0.6$ and 0.9 at $\lambda_{sr} = 1$, $\lambda_{rd} = 1$, $\lambda_{Ir} = 3$, $\lambda_{Id} = 4$, and $\lambda_{Is} = 1$.

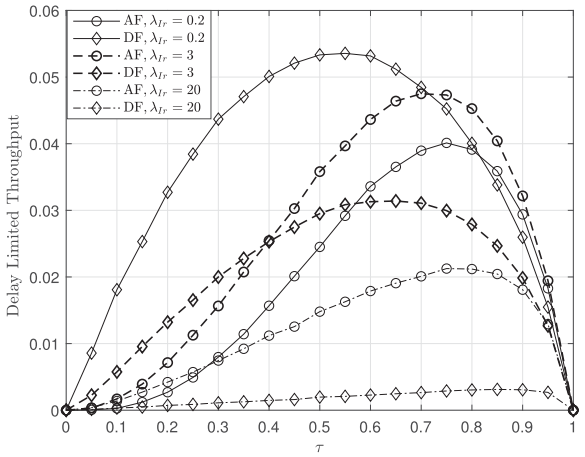

FIGURE 14. Delay limited throughput of mode *III* versus the energy harvesting time τ considering AF and DF protocols for different values of λ_{Ir} at $\lambda_{sr} = 1$, $\lambda_{rd} = 1$, $\lambda_{Id} = 1$, $\lambda_{Is} = 1$, and $P_I = 10$.

are of more practical interest at moderate values of P_I (i.e., $P_I = 1$).

In Fig. 11, we note that Mode I achieves the best throughput performance when $P_I = 0.1$ for all $0 < \tau < 1$. We also observe that Mode II achieves much better than Mode III for all $0 < \tau < 1$. Accordingly, it can be concluded that Mode I and Mode II are of more practical interest at lower values of P_I (i.e., $P_I = 0.1$).

In Fig. 12, depicts the delay-limited throughput of all modes versus the interferer power P_I for two τ values of 0.6 and 0.9. It is clear from this figure that the throughput of Mode I and Mode II decreases with P_I while that of Mode III is invariant with it. We can also notice that Mode III is the best for high P_I values, and hence, it is recommended to be used in such interferer scenarios.

Fig. 13 depicts the optimal delay-limited throughput $\mathcal{R}_{DL}(\tau^*)$ of all Modes against P_I, where $\mathcal{R}_{DL}(\tau^*)$ is being evaluated by solving the optimization problem in (24).

Fig. 14 compares the delay-limited throughput (against τ) of Mode III using the AF protocol with that using the DF protocol considering different values of λ_{Ir} (i.e., different interferer to relay channel conditions).[3] From this figure several novel insightful comparative observations can be obtained. When λ_{Ir} is low (i.e., strong interferer to relay channel), the DF outperforms the AF. This is due to the fact that in the AF relaying, the interference term at the AF relay is amplified along with the desired signal and forwarded to the destination, which results in throughput reduction even though the amount of the relay harvested energy from the same interference is high; while, in the DF protocol, this is not happening but rather the stronger the interference, the more harvested energy at the DF relay and the higher throughput at the destination.

[3]The throughput results using the DF protocol are obtained via simulation. For more details about EH-based DF relaying system set ups, readers can refer to [46].

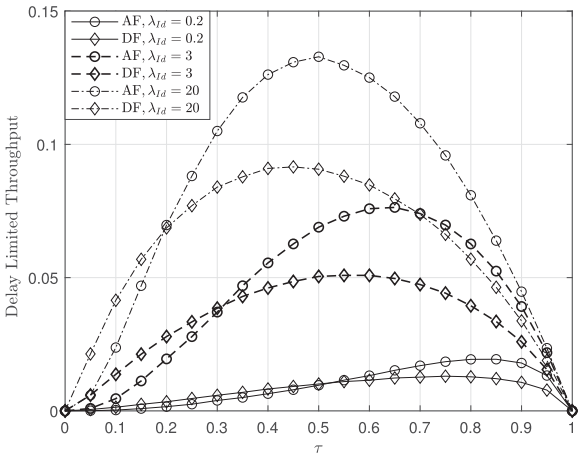

FIGURE 15. Delay limited throughput of mode *III* versus the energy harvesting time τ considering AF and DF protocols for different values of λ_{Id} at $\lambda_{sr} = 1$, $\lambda_{rd} = 1$, $\lambda_{Ir} = 3$, $\lambda_{Is} = 1$, and $P_I = 10$.

Now, increasing λ_{Ir} to medium values (i.e., moderate interferer to relay channel strength, improves the throughput of the AF protocol due to the reduction in the received interference power at the AF relay, and reduces the throughput of the DF protocol due to the reduction in the amount of the harvested energy at the DF relay. Increasing λ_{Ir} more to high values (i.e., extremely weak interferer to relay channel), reduces the overall throughput of both protocols, which is due to the huge reduction in the amount of the harvested energy at the relay. Thus, based on these observations, it would be recommended to employ the DF protocol when the interferer to relay channel is strong and the AF protocol when it is moderate or weak.

Fig. 15 presents the same comparison as in Fig. 14 but for different values of λ_{Id} (i.e., different interferer to destination channel conditions) and moderate λ_{Ir} value of 3. First, it is clear that increasing λ_{Id}, increases the throughput for both protocols, which is due to the reduction of the harmful effect of the interference signal at the destination. It is also clear that, over medium and high τ values, the AF protocol outperforms the DF protocol for all λ_{Id} values, however, the gap between them reduces over the high λ_{Id} values.

VI. CONCLUSION

In this paper, an energy harvesting based Rayleigh fading dual-hop amplify-and-forward relaying system has been considered, where the source and the relay are capable to harvest energy only from an ambient interferer that also corrupts the received signals at both the relay and destination. Under these considerations, the system outage probability has been derived in novel exact analytical expressions and in lower-bound approximate closed-form expressions considering three modes of energy harvesting; mode I (energy is harvested only at the source), mode II (energy is harvested only at the relay), and mode III (energy is harvested simultaneously at both the source and the relay). Subject to fixed source transmission rate, the derived outage probabilities have been directly used to compute the system's delay-limited throughput for the energy harvesting modes under study. Under diverse system and channel parameters, comprehensive numerical and simulation results have been provided to corroborate the conducted analytical derivations and to gain useful insightful observations and comparisons into the system throughput performance. Results have shown that (i) subject to fixed channel conditions, the throughput of mode I and mode II is inversely proportional with the interferer transmit power while that of mode III is independent of it, (ii) subject to fixed interferer transmit power, better interferer to harvesting node channel conditions improves the system throughput while better interferer to receiving node channel conditions degrades the system throughput, (iii) for large interferer transmit power values, mode III offers the best throughput.

APPENDIX A
THEOREM 3.1 PROOF

When energy harvesting is employed at S but not at R, the source transmit power (according to (4)) is given as $P_s^* = \frac{2\zeta_s \tau P_I |h_{Is}|^2}{(1-\tau)}$, while, as in (7), the relay transmit power P_r^* is fixed and equals P_r. Considering this in (13) gives the SIR for this energy harvesting mode as in (25).

$$\mathcal{X}^{\mathrm{I}} = \frac{\frac{2\zeta_s \tau}{(1-\tau)} P_I P_r |h_{Is}|^2 |h_{sr}|^2 |h_{rd}|^2}{P_I P_r |h_{Ir}|^2 |h_{rd}|^2 + \frac{2\zeta_s \tau}{(1-\tau)} P_I^2 |h_{Is}|^2 |h_{sr}|^2 |h_{Id}|^2 + P_I^2 |h_{Ir}|^2 |h_{Id}|^2}. \tag{25}$$

The outage probability at D for energy harvesting mode I, say $P_{\mathrm{out}}^{\mathrm{I}}$, can be obtained by

$$P_{\mathrm{out}}^{\mathrm{I}} = \mathrm{P}_r \left\{ \mathcal{X}^{\mathrm{I}} < \gamma_{\mathrm{th}} \right\}, \tag{26}$$

where $\gamma_{\mathrm{th}} = 2^R - 1$ is a predetermined threshold and R is the transmission data rate at S. Due to the intractable form of the R.V $\mathcal{X}^{\mathrm{I}}$ in (25), we propose to evaluate $P_{\mathrm{out}}^{\mathrm{I}}$ as

$$P_{\mathrm{out}}^{\mathrm{I}} = \int_0^\infty f_{|h_{Is}|^2}(q) \mathrm{P}_r \left\{ \mathcal{X}^{\mathrm{I}} \middle| \left\{ |h_{Is}|^2 = q \right\} < \gamma_{\mathrm{th}} \right\} \mathrm{d}q, \tag{27}$$

where $\mathcal{X}^{\mathrm{I}} \big| \{|h_{Is}|^2 = q\}$ is $\mathcal{X}^{\mathrm{I}}$ conditioned on $|h_{Is}|^2 = q$, which is given as in (28).

$$\mathcal{X}^{\mathrm{I}} \big| \{|h_{Is}|^2 = q\} = \frac{\frac{2\zeta_s \tau}{(1-\tau)} P_I P_r q |h_{sr}|^2 |h_{rd}|^2}{P_I P_r |h_{Ir}|^2 |h_{rd}|^2 + \frac{2\zeta_s \tau}{(1-\tau)} P_I^2 q |h_{sr}|^2 |h_{Id}|^2 + P_I^2 |h_{Ir}|^2 |h_{Id}|^2}. \tag{28}$$

The target now is to determine $\mathrm{P}_r\{\mathcal{X}^{\mathrm{I}} \big| \{|h_{Is}|^2 = q\} < \gamma_{\mathrm{th}}\}$. To attain this, we first define the following R.Vs

$$\mathcal{X}_1 = \frac{2\zeta_s \tau}{(1-\tau)} P_I q |h_{sr}|^2 \tag{29}$$

$$\mathcal{X}_2 = P_r |h_{rd}|^2 \tag{30}$$

$$\Psi_1 = P_I |h_{Ir}|^2 \tag{31}$$

$$\Psi_2 = P_I |h_{Id}|^2. \tag{32}$$

Considering this in (28) gives

$$\mathcal{X}^{\mathrm{I}} \left| \left\{ |h_{Is}|^2 = q \right\} \right. = \frac{\mathcal{X}_1 \mathcal{X}_2}{\Psi_2 \mathcal{X}_1 + \Psi_1 \mathcal{X}_2 + \Psi_1 \Psi_2}. \tag{33}$$

Further, by dividing the numerator and denominator of (33) by $\Psi_1 \Psi_2$, we may have

$$\mathcal{X}^{\mathrm{I}} \left| \left\{ |h_{Is}|^2 = q \right\} \right. = \frac{\frac{\mathcal{X}_1}{\Psi_1} \times \frac{\mathcal{X}_2}{\Psi_2}}{\frac{\mathcal{X}_1}{\Psi_1} + \frac{\mathcal{X}_2}{\Psi_2} + 1}. \tag{34}$$

From (34), we can obtain

$$\mathrm{P}_r \left\{ \mathcal{X}^{\mathrm{I}} \left| \left\{ |h_{Is}|^2 = q \right\} \right. < \gamma_{\mathrm{th}} \right\} = \mathrm{P}_r \left\{ \frac{\frac{\mathcal{X}_1}{\Psi_1} \times \frac{\mathcal{X}_2}{\Psi_2}}{\frac{\mathcal{X}_1}{\Psi_1} + \frac{\mathcal{X}_2}{\Psi_2} + 1} < \gamma_{\mathrm{th}} \right\}, \tag{35}$$

which can be computed as in (36).

$$\begin{aligned} &\mathrm{P}_r \left\{ \mathcal{X}^{\mathrm{I}} \left| \left\{ |h_{Is}|^2 = q \right\} \right. < \gamma_{\mathrm{th}} \right\} \\ &= 1 - \int_{\gamma_{\mathrm{th}}}^{\infty} f_{\frac{\mathcal{X}_1}{\Psi_1}}(x) \mathrm{d}x + \int_{\gamma_{\mathrm{th}}}^{\infty} f_{\frac{\mathcal{X}_1}{\Psi_1}}(x) \mathrm{P}_r \left\{ \frac{\mathcal{X}_2}{\Psi_2} < \frac{(x+1)\gamma_{\mathrm{th}}}{x - \gamma_{\mathrm{th}}} \right\} \mathrm{d}x. \end{aligned} \tag{36}$$

According to (1) and (29) to (32), we have

$$\mathcal{X}_1 \sim \exp\left(0, \frac{(1-\tau)\lambda_{sr}}{2\zeta_s \tau P_I q}\right) \tag{37}$$

$$\mathcal{X}_2 \sim \exp\left(0, \frac{\lambda_{rd}}{P_r}\right) \tag{38}$$

$$\Psi_1 \sim \exp\left(0, \frac{\lambda_{Ir}}{P_I}\right) \tag{39}$$

$$\Psi_2 \sim \exp\left(0, \frac{\lambda_{Id}}{P_I}\right). \tag{40}$$

Based on this, and with the help of [53], the PDF and CDF of $\frac{\mathcal{X}_1}{\Psi_1}$ and $\frac{\mathcal{X}_2}{\Psi_2}$ can be obtained respectively as

$$f_{\frac{\mathcal{X}_1}{\Psi_1}}(x) = \frac{2\zeta_s \tau \lambda_{Ir} q}{(1-\tau)\lambda_{sr} \left(x + \frac{2\zeta_s \tau \lambda_{Ir} q}{(1-\tau)\lambda_{sr}} \right)^2} \tag{41}$$

$$F_{\frac{\mathcal{X}_1}{\Psi_1}}(x) = \frac{x}{x + \frac{2\zeta_s \tau \lambda_{Ir} q}{(1-\tau)\lambda_{sr}}} \tag{42}$$

$$f_{\frac{\mathcal{X}_2}{\Psi_2}}(x) = \frac{P_r \lambda_{Id} q}{P_I \lambda_{rd} \left(x + \frac{P_r \lambda_{Id} q}{P_I \lambda_{rd}} \right)^2} \tag{43}$$

and

$$F_{\frac{\mathcal{X}_2}{\Psi_2}}(x) = \frac{x}{x + \frac{P_r \lambda_{Id}}{P_I \lambda_{rd}}}. \tag{44}$$

Substituting (41) and (44) into (36), solving for the first integral, and doing some simplifications gives (45). Simplifying with $z = x - \gamma_{\mathrm{th}}$ gives (46).

$$\begin{aligned} \mathrm{P}_r \left\{ \mathcal{X}^{\mathrm{I}} \left| \left\{ |h_{Is}|^2 = q \right\} \right. < \gamma_{\mathrm{th}} \right\} &= \frac{\gamma_{\mathrm{th}}}{\gamma_{\mathrm{th}} + \frac{2\zeta_s \tau \lambda_{Ir} q}{(1-\tau)\lambda_{sr}}} \\ &+ \int_{\gamma_{\mathrm{th}}}^{\infty} \frac{(x+1)\gamma_{\mathrm{th}}}{(x+1)\gamma_{\mathrm{th}} + \frac{P_r \lambda_{Id}}{P_I \lambda_{rd}}(x - \gamma_{\mathrm{th}})} \\ &\times \frac{2\zeta_s \tau \lambda_{Ir} q}{(1-\tau)\lambda_{sr} \left(x + \frac{2\zeta_s \tau \lambda_{Ir} q}{(1-\tau)\lambda_{sr}} \right)^2} \mathrm{d}x. \end{aligned} \tag{45}$$

$$\begin{aligned} \mathrm{P}_r \left\{ \mathcal{X}^{\mathrm{I}} \left| \left\{ |h_{Is}|^2 = q \right\} \right. < \gamma_{\mathrm{th}} \right\} &= \frac{\gamma_{\mathrm{th}}}{\gamma_{\mathrm{th}} + \frac{2\zeta_s \tau \lambda_{Ir} q}{(1-\tau)\lambda_{sr}}} \\ &+ \int_{0}^{\infty} \frac{\gamma_{\mathrm{th}} z + \gamma_{\mathrm{th}}(\gamma_{\mathrm{th}} + 1)}{(\gamma_{\mathrm{th}} + \frac{P_r \lambda_{Id}}{P_I \lambda_{rd}})z + \gamma_{\mathrm{th}}(\gamma_{\mathrm{th}} + 1)} \\ &\times \frac{2\zeta_s \tau \lambda_{Ir} q}{(1-\tau)\lambda_{sr} \left(z + \gamma_{\mathrm{th}} + \frac{2\zeta_s \tau \lambda_{Ir} q}{(1-\tau)\lambda_{sr}} \right)^2} \mathrm{d}z. \end{aligned} \tag{46}$$

$$\begin{aligned} \mathrm{P}_r \left\{ \mathcal{X}^{\mathrm{I}} \left| \left\{ |h_{Is}|^2 = q \right\} \right. < \gamma_{\mathrm{th}} \right\} &= \frac{\gamma_{\mathrm{th}}}{\gamma_{\mathrm{th}} + \frac{2\zeta_s \tau \lambda_{Ir} q}{(1-\tau)\lambda_{sr}}} \\ &+ \frac{\gamma_{\mathrm{th}}^2 (\gamma_{\mathrm{th}} + 1) B(2,1)}{\left(\gamma_{\mathrm{th}} + \frac{P_r \lambda_{Id}}{P_I \lambda_{rd}} \right)^2} \frac{\frac{2\zeta_s \tau \lambda_{Ir}}{(1-\tau)\lambda_{sr}} q}{\left(\frac{2\zeta_s \tau \lambda_{Ir}}{(1-\tau)\lambda_{sr}} q + \gamma_{\mathrm{th}} \right)^2} \\ &\times F\left(2, 2; 3; 1 - \frac{\gamma_{\mathrm{th}}(\gamma_{\mathrm{th}} + 1)}{\left(\gamma_{\mathrm{th}} + \frac{P_r \lambda_{Id}}{P_I \lambda_{rd}} \right) \left(\frac{2\zeta_s \tau \lambda_{Ir}}{(1-\tau)\lambda_{sr}} q + \gamma_{\mathrm{th}} \right)} \right) \\ &+ \frac{\gamma_{\mathrm{th}}^2 (\gamma_{\mathrm{th}} + 1)^2 B(1,2)}{\left(\gamma_{\mathrm{th}} + \frac{P_r \lambda_{Id}}{P_I \lambda_{rd}} \right)^2} \frac{\frac{2\zeta_s \tau \lambda_{Ir}}{(1-\tau)\lambda_{sr}} q}{\left(\frac{2\zeta_s \tau \lambda_{Ir}}{(1-\tau)\lambda_{sr}} q + \gamma_{\mathrm{th}} \right)^2} \\ &\times F\left(2, 1; 3; 1 - \frac{\gamma_{\mathrm{th}}(\gamma_{\mathrm{th}} + 1)}{\left(\gamma_{\mathrm{th}} + \frac{P_r \lambda_{Id}}{P_I \lambda_{rd}} \right) \left(\frac{2\zeta_s \tau \lambda_{Ir}}{(1-\tau)\lambda_{sr}} q + \gamma_{\mathrm{th}} \right)} \right). \end{aligned} \tag{47}$$

By solving the integral in (46) with the help of [52, Eq. (3.259-3)], we can obtain the ultimate exact expression for $\mathrm{P}_r\{\mathcal{X}^{\mathrm{I}} | \{|h_{Is}|^2 = q\} < \gamma_{\mathrm{th}}\}$ as in (47) where $B(\cdot, \cdot)$ is the Beta function [52, 8.380-1] and $F(\alpha, \beta; \gamma; z)$ is the hypergeometric function [52, (9.100)]. Now, by substituting (47) and (1) (with $ab = Is$) into (27), we may have $P_{\mathrm{out}}^{\mathrm{I}}$ as in (48) shown at the bottom of the next page. With the help of [52, Eq. (3.352-4)], we can have I_1 as

$$\begin{aligned} I_1 = &- \frac{\lambda_{Is} \gamma_{\mathrm{th}} (1-\tau)\lambda_{sr}}{2\zeta_s \tau \lambda_{Ir}} e^{\left(\frac{(1-\tau)\lambda_{sr} \lambda_{Is} \gamma_{\mathrm{th}}}{2\zeta_s \tau \lambda_{Ir}} \right)} \\ &\times \mathrm{Ei}\left(- \frac{(1-\tau)\lambda_{sr} \lambda_{Is} \gamma_{\mathrm{th}}}{2\zeta_s \tau \lambda_{Ir}} \right), \end{aligned} \tag{49}$$

With regard to I_2 and I_3, we are unaware of a closed-form solution for them even in well-known integral tables. Thus, our proposition to solve for them is as follows. First, making use of the hypergeometric function series expansion [52, Eq. (9.14.1)]

$$F(\alpha, \beta; \gamma; z) = \sum_{n=0}^{\infty} \frac{(\alpha)_n (\beta)_n}{(\gamma)_n} \frac{z^n}{n!} \tag{50}$$

in I_2 given in (48) along with some arrangements yields

$$I_2 = \sum_{n=0}^{\infty} \frac{(2)_n (2)_n}{(3)_n n!} \int_0^{\infty} \frac{\frac{2\zeta_s \tau \lambda_{Ir}}{(1-\tau)\lambda_{sr}} q}{\left(\frac{2\zeta_s \tau \lambda_{Ir}}{(1-\tau)\lambda_{sr}} q + \gamma_{\text{th}}\right)^{n+2}} \times \left(\frac{2\zeta_s \tau \lambda_{Ir}}{(1-\tau)\lambda_{sr}} q + \gamma_{\text{th}} - \frac{\gamma_{\text{th}}(\gamma_{\text{th}}+1)}{\gamma_{\text{th}} + \frac{P_r \lambda_{Id}}{P_I \lambda_{rd}}}\right)^n e^{-\lambda_{Is} q} \mathrm{d}q, \tag{51}$$

where $(a)_n = \frac{\Gamma(a+n)}{\Gamma(a)}$ denotes for the Pochhammer symbol. Expanding

$$\left(\frac{2\zeta_s \tau \lambda_{Ir}}{(1-\tau)\lambda_{sr}} q + \gamma_{\text{th}} - \frac{\gamma_{\text{th}}(\gamma_{\text{th}}+1)}{\gamma_{\text{th}} + \frac{P_r \lambda_{Id}}{P_I \lambda_{rd}}}\right)^n$$

using the power series expansion gives

$$I_2 = \sum_{n=0}^{\infty} \frac{(2)_n (2)_n}{(3)_n n!} \sum_{k=0}^{n} \binom{n}{k} \left(\frac{2\zeta_s \tau \lambda_{Ir}}{(1-\tau)\lambda_{sr}}\right)^{k+1} \times \left(\gamma_{\text{th}} - \frac{\gamma_{\text{th}}(\gamma_{\text{th}}+1)}{\gamma_{\text{th}} + \frac{P_r \lambda_{Id}}{P_I \lambda_{rd}}}\right)^{n-k} \int_0^{\infty} \frac{q^k e^{-\lambda_{Is} q}}{\left(\frac{2\zeta_s \tau \lambda_{Ir}}{(1-\tau)\lambda_{sr}} q + \gamma_{\text{th}}\right)^{n+2}} \mathrm{d}q. \tag{52}$$

Solving for the last integral in (52) using [54, Eq. (2.3.6.9)] ultimately gives I_2 as

$$I_2 = \sum_{n=0}^{\infty} \frac{(2)_n (2)_n}{(3)_n n!} \sum_{k=0}^{n} \binom{n}{k} \left(\frac{2\zeta_s \tau \lambda_{Ir}}{(1-\tau)\lambda_{sr}}\right)^{k-n-1} \left(\gamma_{\text{th}} - \frac{\gamma_{\text{th}}(\gamma_{\text{th}}+1)}{\gamma_{\text{th}} + \frac{P_r \lambda_{Id}}{P_I \lambda_{rd}}}\right)^{n-k} \Gamma(k+2) \left(\frac{(1-\tau)\lambda_{sr}\gamma_{\text{th}}}{2\zeta_s \tau \lambda_{Ir}}\right)^{k-n} \times \Psi\left(k+2, 1+k-n; \frac{(1-\tau)\lambda_{sr}\lambda_{Is}\gamma_{\text{th}}}{2\zeta_s \tau \lambda_{Ir}}\right), \tag{53}$$

where $\Psi(\alpha, \beta, \gamma)$ is the Tricomi hypergeometric function [52, 9.211-4.8]. Similarly, I_3 can be obtained by

$$I_3 = \sum_{n=0}^{\infty} \frac{(2)_n (1)_n}{(3)_n n!} \sum_{k=0}^{n} \binom{n}{k} \left(\frac{2\zeta_s \tau \lambda_{Ir}}{(1-\tau)\lambda_{sr}}\right)^{k-n-1} \left(\gamma_{\text{th}} - \frac{\gamma_{\text{th}}(\gamma_{\text{th}}+1)}{\gamma_{\text{th}} + \frac{P_r \lambda_{Id}}{P_I \lambda_{rd}}}\right)^{n-k} \Gamma(k+2) \left(\frac{(1-\tau)\lambda_{sr}\gamma_{\text{th}}}{2\zeta_s \tau \lambda_{Ir}}\right)^{k-n} \times \Psi\left(k+2, 1+k-n; \frac{(1-\tau)\lambda_{sr}\lambda_{Is}\gamma_{\text{th}}}{2\zeta_s \tau \lambda_{Ir}}\right) \tag{54}$$

Finally, substituting (49), (53) and (54) into (48) along with some simplifications and manipulations gives (25), which completes the proof.

APPENDIX B
THEOREM 3.2 PROOF

First, the conditional SIR in (34) can be approximated by the following tight upper bound

$$\mathcal{X}^{\text{I}} \left| \{|h_{Is}|^2 = q\} \right. \leq \mathcal{X}^{\text{I}}_{\text{up}} \left| \{|h_{Is}|^2 = q\} \right. = \min\left(\frac{\mathcal{X}_1}{\Psi_1}, \frac{\mathcal{X}_2}{\Psi_2}\right). \tag{55}$$

As $\frac{\mathcal{X}_1}{\Psi_1}$ and $\frac{\mathcal{X}_2}{\Psi_2}$ are two independent R.Vs, we can have

$$\mathrm{P}_r\left\{\mathcal{X}^{\text{I}}_{\text{up}} \left| \{|h_{Is}|^2 = q\} \right. < \gamma_{\text{th}}\right\} = 1 - \left[1 - F_{\frac{\mathcal{X}_1}{\Psi_1}}(\gamma_{\text{th}})\right] \times \left[1 - F_{\frac{\mathcal{X}_2}{\Psi_2}}(\gamma_{\text{th}})\right]. \tag{56}$$

Substituting (42) and (44) into (56) gives

$$\mathrm{P}_r\left\{\mathcal{X}^{\text{I}}_{\text{up}} \left| \{|h_{Is}|^2 = q\} \right. < \gamma_{\text{th}}\right\} = 1 - \left[\frac{P_r \lambda_{Id}}{P_I \lambda_{rd}\gamma_{\text{th}} + P_r \lambda_{Id}}\right] \times \left[\frac{\frac{2\zeta_s \tau \lambda_{Ir}}{(1-\tau)\lambda_{sr}} q}{\frac{2\zeta_s \tau \lambda_{Ir}}{(1-\tau)\lambda_{sr}} q + \gamma_{\text{th}}}\right]. \tag{57}$$

$$P^{\text{I}}_{\text{out}} = \underbrace{\int_0^{\infty} \frac{\lambda_{Is}\gamma_{\text{th}}}{\gamma_{\text{th}} + \frac{2\zeta_s \tau \lambda_{Ir} q}{(1-\tau)\lambda_{sr}}} e^{-\lambda_{Is} q} \mathrm{d}q}_{I_1} + \frac{\lambda_{Is}\gamma_{\text{th}}^2(\gamma_{\text{th}}+1)B(2,1)}{\left(\gamma_{\text{th}} + \frac{P_r \lambda_{Id}}{P_I \lambda_{rd}}\right)^2} \times \underbrace{\int_0^{\infty} \frac{\frac{2\zeta_s \tau \lambda_{Ir}}{(1-\tau)\lambda_{sr}} q e^{-\lambda_{Is} q}}{\left(\frac{2\zeta_s \tau \lambda_{Ir}}{(1-\tau)\lambda_{sr}} q + \gamma_{\text{th}}\right)^2} F\left(2, 2; 3; 1 - \frac{\gamma_{\text{th}}(\gamma_{\text{th}}+1)}{\left(\gamma_{\text{th}} + \frac{P_r \lambda_{Id}}{P_I \lambda_{rd}}\right)\left(\frac{2\zeta_s \tau \lambda_{Ir}}{(1-\tau)\lambda_{sr}} q + \gamma_{\text{th}}\right)}\right) \mathrm{d}q}_{I_2} + \frac{\lambda_{Is}\gamma_{\text{th}}^2(\gamma_{\text{th}}+1)^2 B(1,2)}{\left(\gamma_{\text{th}} + \frac{P_r \lambda_{Id}}{P_I \lambda_{rd}}\right)^2} \times \underbrace{\int_0^{\infty} \frac{\frac{2\zeta_s \tau \lambda_{Ir}}{(1-\tau)\lambda_{sr}} q e^{-\lambda_{Is} q}}{\left(\frac{2\zeta_s \tau \lambda_{Ir}}{(1-\tau)\lambda_{sr}} q + \gamma_{\text{th}}\right)^2} F\left(2, 1; 3; 1 - \frac{\gamma_{\text{th}}(\gamma_{\text{th}}+1)}{\left(\gamma_{\text{th}} + \frac{P_r \lambda_{Id}}{P_I \lambda_{rd}}\right)\left(\frac{2\zeta_s \tau \lambda_{Ir}}{(1-\tau)\lambda_{sr}} q + \gamma_{\text{th}}\right)}\right) \mathrm{d}q}_{I_3} \tag{48}$$

Now, considering the conditional upper bound SIR in (57) along with (1) (with $ab = Is$) into (27) gives the following lower bound for $P_{\text{out}}^{\text{I}}$

$$P_{\text{out,Low}}^{\text{I}} = 1 - \left[\frac{P_r\lambda_{Id}}{P_I\lambda_{rd}\gamma_{\text{th}} + P_r\lambda_{Id}}\right] \times \underbrace{\int_0^{\infty} \lambda_{Is} e^{-\lambda_{Is}q}\left[\frac{\frac{2\zeta_s\tau\lambda_{Ir}}{(1-\tau)\lambda_{sr}}q}{\frac{2\zeta_s\tau\lambda_{Ir}}{(1-\tau)\lambda_{sr}}q + \gamma_{\text{th}}}\right]\text{d}q}_{I_3}. \quad (58)$$

Solving for I_3 using [54, Eq. (2.3.6.9)] ultimately gives $P_{\text{out,Low}}^{\text{I}}$ as in (16).

APPENDIX C
THEOREM 3.3 PROOF

With energy harvesting is employed only at R, the system SIR can be obtained from (13) by setting $P_s^* = P_s$ (as in (4)) and $P_r^* = \frac{2\zeta_r\tau P_I|h_{Ir}|^2}{(1-\tau)}$ (as in (7)), which gives (59).

$$\mathcal{X}^{\text{II}} = \frac{\frac{2\zeta_r\tau}{(1-\tau)}P_IP_s|h_{Ir}|^2|h_{sr}|^2|h_{rd}|^2}{\frac{2\zeta_r\tau}{(1-\tau)}P_I^2|h_{Ir}|^4|h_{rd}|^2 + P_IP_s|h_{sr}|^2|h_{Id}|^2 + P_I^2|h_{Ir}|^2|h_{Id}|^2}. \quad (59)$$

Using $\mathcal{X}^{\text{II}}$, the outage probability for energy harvesting mode II, say $P_{\text{out}}^{\text{II}}$, can be computed by

$$P_{\text{out}}^{\text{II}} = \text{P}_r\left\{\mathcal{X}^{\text{II}} < \gamma_{\text{th}}\right\}. \quad (60)$$

To simplify the problem of obtaining $\text{P}_r\{\mathcal{X}^{\text{II}} < \gamma_{\text{th}}\}$, we need first to re-present $\mathcal{X}^{\text{II}}$ in more helpful form, which can be done as follows. First, dividing the numerator and the denominator of (59) by $|h_{Ir}|^2$ may give

$$\mathcal{X}^{\text{II}} = \frac{\frac{2\zeta_r\tau}{(1-\tau)}P_IP_s|h_{sr}|^2|h_{rd}|^2}{\frac{2\zeta_r\tau}{(1-\tau)}P_I^2|h_{Ir}|^2|h_{rd}|^2 + P_IP_s\frac{|h_{sr}|^2|h_{Id}|^2}{|h_{Ir}|^2} + P_I^2|h_{Id}|^2}. \quad (61)$$

By defining

$$\mathcal{L}_1 = P_s|h_{sr}|^2 \quad (62)$$

$$\mathcal{Y}_2 = \frac{2\zeta_r\tau}{(1-\tau)}P_I|h_{rd}|^2 \quad (63)$$

$$\Phi_2 = P_I\frac{|h_{Id}|^2}{|h_{Ir}|^2}. \quad (64)$$

we may write

$$\mathcal{X}^{\text{II}} = \frac{\mathcal{L}_1\mathcal{Y}_2}{\Phi_2\mathcal{L}_1 + \Psi_1\mathcal{Y}_2 + \Psi_1\Phi_2}, \quad (65)$$

where Ψ_1 is defined in (31). Now, dividing the numerator and denominator of (65) by $\Psi_1\Phi_2$ gives

$$\mathcal{X}^{\text{II}} = \frac{\frac{\mathcal{L}_1}{\Psi_1} \times \frac{\mathcal{Y}_2}{\Phi_2}}{\frac{\mathcal{L}_1}{\Psi_1} + \frac{\mathcal{Y}_2}{\Phi_2} + 1}. \quad (66)$$

From (66), we can now have

$$\text{P}_r\left\{\mathcal{X}^{\text{II}} < \gamma_{\text{th}}\right\} = \underbrace{1 - \int_{\gamma_{\text{th}}}^{\infty} f_{\frac{\mathcal{L}_1}{\Psi_1}}(x)\text{d}x}_{\triangleq F_{\frac{\mathcal{L}_1}{\Psi_1}}(\gamma_{\text{th}})} + \int_{\gamma_{\text{th}}}^{\infty} f_{\frac{\mathcal{L}_1}{\Psi_1}}(x)\underbrace{\text{P}_r\left\{\frac{\mathcal{Y}_2}{\Phi_2} < \frac{(x+1)\gamma_{\text{th}}}{x-\gamma_{\text{th}}}\right\}}_{\triangleq F_{\frac{\mathcal{Y}_2}{\Phi_2}}\left(\frac{(x+1)\gamma_{\text{th}}}{x-\gamma_{\text{th}}}\right)}\text{d}x, \quad (67)$$

where

$$f_{\frac{\mathcal{L}_1}{\Psi_1}}(x) = \frac{\frac{\lambda_{Ir}P_s}{\lambda_{sr}P_I}}{\left(x + \frac{\lambda_{Ir}P_s}{\lambda_{sr}P_I}\right)^2} \quad (68)$$

$$F_{\frac{\mathcal{L}_1}{\Psi_1}}(x) = \frac{x}{x + \frac{\lambda_{Ir}P_s}{\lambda_{sr}P_I}}. \quad (69)$$

and the CDF $F_{\frac{\mathcal{Y}_2}{\Phi_2}}(u)$ is given by the following proposition.

Proposition C.1:

$$F_{\frac{\mathcal{Y}_2}{\Phi_2}}(u) = -\frac{(1-\tau)\lambda_{rd}\lambda_{Ir}}{2\zeta_r\tau\lambda_{Id}}u\, e^{\left(\frac{(1-\tau)\lambda_{rd}\lambda_{Ir}}{2\zeta_r\tau\lambda_{Id}}u\right)} \times \text{Ei}\left(-\frac{(1-\tau)\lambda_{rd}\lambda_{Ir}}{2\zeta_r\tau\lambda_{Id}}u\right). \quad (70)$$

Proof:

$$F_{\frac{\mathcal{Y}_2}{\Phi_2}}(u) = \text{P}_r\left\{\frac{\mathcal{Y}_2}{\Phi_2} < u\right\} = \text{P}_r\left\{\frac{2\zeta_r\tau}{(1-\tau)}|h_{rd}|^2\frac{|h_{Ir}|^2}{|h_{Id}|^2} < u\right\}. \quad (71)$$

By defining $\Lambda = \frac{2\zeta_r\tau}{(1-\tau)}|h_{rd}|^2$, which is $\exp(0, \frac{(1-\tau)\lambda_{rd}}{2\zeta_r\tau})$, we can write

$$F_{\frac{\mathcal{Y}_2}{\Phi_2}}(u) = \int_0^{\infty} f_{\Lambda}(g)\text{P}_r\left\{g\frac{|h_{Ir}|^2}{|h_{Id}|^2} < u\right\}\text{d}g = \int_0^{\infty}\frac{(1-\tau)\lambda_{rd}}{2\zeta_r\tau}e^{-\frac{(1-\tau)\lambda_{rd}}{2\zeta_r\tau}g}\frac{u}{u + g\frac{\lambda_{Id}}{\lambda_{Ir}}}\text{d}g. \quad (72)$$

By solving for the integral in (72) with the help of [3.352-4] we can obtain (70), which completes the proof. ■

Now, considering (68), (69) and (70) with $u = \frac{(x+1)\gamma_{\text{th}}}{x-\gamma_{\text{th}}}$ in (67) yields (73).

$$\text{P}_r\left\{\mathcal{X}^{\text{II}} < \gamma_{\text{th}}\right\} = \frac{\gamma_{\text{th}}}{\gamma_{\text{th}} + \frac{\lambda_{Ir}P_s}{\lambda_{sr}P_I}} - \int_{\gamma_{\text{th}}}^{\infty}\frac{\frac{\lambda_{Ir}P_s}{\lambda_{sr}P_I}}{\left(x + \frac{\lambda_{Ir}P_s}{\lambda_{sr}P_I}\right)^2}\frac{(1-\tau)\lambda_{rd}\lambda_{Ir}}{2\zeta_r\tau\lambda_{Id}} \times \frac{(x+1)\gamma_{\text{th}}}{x-\gamma_{\text{th}}}\, e^{\left(\frac{(1-\tau)\lambda_{rd}\lambda_{Ir}}{2\zeta_r\tau\lambda_{Id}}\frac{(x+1)\gamma_{\text{th}}}{x-\gamma_{\text{th}}}\right)} \times \text{Ei}\left(-\frac{(1-\tau)\lambda_{rd}\lambda_{Ir}}{2\zeta_r\tau\lambda_{Id}}\frac{(x+1)\gamma_{\text{th}}}{x-\gamma_{\text{th}}}\right)\text{d}x. \quad (73)$$

Letting $z = x - \gamma_{\text{th}}$ gives (17).

APPENDIX D
THEOREM 3.4 PROOF

In analogy to (55), the conditional SIR in (66) can be tightly approximated using the following upper bound

$$\mathcal{X}^{\text{II}} \leq \mathcal{X}^{\text{II}}_{\text{up}} = \min\left(\frac{\mathcal{L}_1}{\Psi_1}, \frac{\mathcal{Y}_2}{\Phi_2}\right). \tag{74}$$

Thus, the lower bound outage probability for mode II can be computed as

$$P^{\text{II}}_{\text{out,Low}} = \text{P}_r\left\{\mathcal{X}^{\text{II}}_{\text{up}} < \gamma_{\text{th}}\right\} = \text{P}_r\left\{\min\left(\frac{\mathcal{L}_1}{\Psi_1}, \frac{\mathcal{Y}_2}{\Phi_2}\right) < \gamma_{\text{th}}\right\}. \tag{75}$$

Notice that $\frac{\mathcal{L}_1}{\Psi_1}$ and $\frac{\mathcal{X}_2}{\Psi_2}$ are not statistically independent because they share the same random variable $|h_{Ir}|^2$, and thus, $P^{\text{II}}_{\text{out,Low}}$ cannot be obtained using the formula in (56). However, our proposition to obtain it as follows. First we may write

$$P^{\text{II}}_{\text{out,Low}} = 1 - \text{P}_r\left\{\frac{\mathcal{L}_1}{\Psi_1} > \gamma_{\text{th}} \bigcap \frac{\mathcal{Y}_2}{\Phi_2} > \gamma_{\text{th}}\right\}. \tag{76}$$

Conditioned on $|h_{Ir}|^2 = f$, we have

$$P^{\text{II}}_{\text{out,Low}}\left|\left\{|h_{Ir}|^2 = f\right\}\right. = 1 - \text{P}_r\left\{\frac{\mathcal{L}_1}{\Psi_1}\middle|\left\{|h_{Ir}|^2 = f\right\} > \gamma_{\text{th}}\right\} \times \text{P}_r\left\{\frac{\mathcal{Y}_2}{\Phi_2}\middle|\left\{|h_{Ir}|^2 = f\right\} > \gamma_{\text{th}}\right\}. \tag{77}$$

Then $P^{\text{II}}_{\text{out,Low}}$ can be obtained from $P^{\text{II}}_{\text{out,Low}}\left|\{|h_{Ir}|^2 = f\right.\}$ as

$$\begin{aligned} P^{\text{II}}_{\text{out,Low}} &= 1 - \int_0^\infty \text{P}_r\left\{\frac{\mathcal{L}_1}{\Psi_1}\middle|\left\{|h_{Ir}|^2 = f\right\} > \gamma_{\text{th}}\right\} \\ &\quad \times \text{P}_r\left\{\frac{\mathcal{Y}_2}{\Phi_2}\middle|\left\{|h_{Ir}|^2 = f\right\} > \gamma_{\text{th}}\right\} f_{|h_{Ir}|^2}(f)df \\ &= 1 - \int_0^\infty \left[1 - F_{\frac{\mathcal{L}_1}{\Psi_1}\left|\{|h_{Ir}|^2=f\right\}}(\gamma_{\text{th}})\right] \\ &\quad \times \left[1 - F_{\frac{\mathcal{Y}_2}{\Phi_2}\left|\{|h_{Ir}|^2=f\right\}}(\gamma_{\text{th}})\right] f_{|h_{Ir}|^2}(f)df. \end{aligned} \tag{78}$$

It can be shown that

$$F_{\frac{\mathcal{L}_1}{\Psi_1}\left|\{|h_{Ir}|^2=f\right\}}(\gamma_{\text{th}}) = 1 - e^{-\frac{\lambda_{sr}P_I}{P_s}\gamma_{\text{th}}f} \tag{79}$$

and

$$F_{\frac{\mathcal{Y}_2}{\Phi_2}\left|\{|h_{Ir}|^2=f\right\}}(\gamma_{\text{th}}) = \frac{\gamma_{\text{th}}}{\gamma_{\text{th}} + \frac{\lambda_{Id}2\zeta_r\tau}{(1-\tau)\lambda_{rd}}f}. \tag{80}$$

Considering (1) with $ab = Ir$, (79) and (80) into (78) yields

$$P^{\text{II}}_{\text{out,Low}} = 1 - \int_0^\infty \lambda_{Ir} e^{-\left[\lambda_{Ir} + \frac{\lambda_{sr}P_I\gamma_{\text{th}}}{P_s}\right]f} \frac{\frac{\lambda_{Id}2\zeta_r\tau}{(1-\tau)\lambda_{rd}}f}{\gamma_{\text{th}} + \frac{\lambda_{Id}2\zeta_r\tau}{(1-\tau)\lambda_{rd}}f} df. \tag{81}$$

Solving for the last integral in (81) using [54, Eq. (2.3.6.9)] along with some simplifications gives (19).

APPENDIX E
THEOREM 3.5 PROOF

With energy harvesting is employed at both S and R, the system SIR can be obtained from (13) by setting $P^*_s = \frac{2\zeta_s\tau P_I|h_{Is}|^2}{(1-\tau)}$ (as in (4)) and $P^*_r = \frac{2\zeta_r\tau P_I|h_{Ir}|^2}{(1-\tau)}$ (as in (7)), which gives (82) shown at the bottom of this page. Now, the outage probability for this energy harvesting Mode, say $P^{\text{III}}_{\text{out}}$, can be obtained as

$$P^{\text{III}}_{\text{out}} = \text{P}_r\left\{\mathcal{X}^{\text{III}} < \gamma_{\text{th}}\right\}. \tag{83}$$

However, to assist tractability, we manipulate it to be computed by

$$P^{\text{III}}_{\text{out}} = \int_0^\infty f_{|h_{Is}|^2}(q)\text{P}_r\left\{\mathcal{X}^{\text{III}}\middle|\left\{|h_{Is}|^2 = q\right\} < \gamma_{\text{th}}\right\} \text{d}q, \tag{84}$$

where the conditional SIR $\mathcal{X}^{\text{III}}\left|\{|h_{Is}|^2 = q\right.\}$ is given by (85).

$$\mathcal{X}^{\text{III}}\left|\left\{|h_{Is}|^2 = q\right\}\right. = \frac{\frac{2\zeta_s\tau}{(1-\tau)}\frac{2\zeta_r\tau}{(1-\tau)}P_I^2 q|h_{Ir}|^2|h_{sr}|^2|h_{rd}|^2}{\frac{2\zeta_r\tau}{(1-\tau)}P_I^2|h_{Ir}|^4|h_{rd}|^2 + \frac{2\zeta_s\tau}{(1-\tau)}P_I^2 q|h_{sr}|^2|h_{Id}|^2 + P_I^2|h_{Ir}|^2|h_{Id}|^2}. \tag{85}$$

By dividing the numerator and the denominator of (85) by $|h_{Ir}|^2$ along with some arrangements we obtain

$$\mathcal{X}^{\text{III}}\left|\left\{|h_{Is}|^2 = q\right\}\right. = \frac{\mathcal{X}_1\mathcal{Y}_2}{\Phi_2\mathcal{X}_1 + \Psi_1\mathcal{Y}_2 + \Psi_1\Phi_2}, \tag{86}$$

where $\mathcal{X}_1$, Ψ_1, $\mathcal{Y}_2$ and Φ_2 are defined in (29), (31), (63) and (64), respectively. Dividing the numerator and denominator of (86) by $\Psi_1\Phi_2$ gives

$$\mathcal{X}^{\text{III}}\left|\left\{|h_{Is}|^2 = q\right\}\right. = \frac{\frac{\mathcal{X}_1}{\Psi_1} \times \frac{\mathcal{Y}_2}{\Phi_2}}{\frac{\mathcal{X}_1}{\Psi_1} + \frac{\mathcal{Y}_2}{\Phi_2} + 1}. \tag{87}$$

$$\mathcal{X}^{\text{III}} = \frac{\frac{2\zeta_s\tau}{(1-\tau)}\frac{2\zeta_r\tau}{(1-\tau)}P_I^2|h_{Is}|^2|h_{Ir}|^2|h_{sr}|^2|h_{rd}|^2}{\frac{2\zeta_r\tau}{(1-\tau)}P_I^2|h_{Ir}|^4|h_{rd}|^2 + \frac{2\zeta_s\tau}{(1-\tau)}P_I^2|h_{Is}|^2|h_{sr}|^2|h_{Id}|^2 + P_I^2|h_{Ir}|^2|h_{Id}|^2} \tag{82}$$

Then

$$\begin{aligned}\mathrm{P}_r\left\{\mathcal{X}^{\mathrm{III}}\middle|\left\{|h_{Is}|^2=q\right\}<\gamma_{\mathrm{th}}\right\}&=\mathrm{P}_r\left\{\frac{\frac{\mathcal{X}_1}{\Psi_1}\times\frac{\mathcal{Y}_2}{\Phi_2}}{\frac{\mathcal{X}_1}{\Psi_1}+\frac{\mathcal{Y}_2}{\Phi_2}+1}<\gamma_{\mathrm{th}}\right\}\\&=1-\int_{\gamma_{\mathrm{th}}}^{\infty}f_{\frac{\mathcal{X}_1}{\Psi_1}}(x)\mathrm{d}x\\&\quad+\int_{\gamma_{\mathrm{th}}}^{\infty}f_{\frac{\mathcal{X}_1}{\Psi_1}}(x)\\&\quad\times\mathrm{P}_r\left\{\frac{\mathcal{Y}_2}{\Phi_2}<\frac{(x+1)\gamma_{\mathrm{th}}}{x-\gamma_{\mathrm{th}}}\right\}\mathrm{d}x.\end{aligned}\tag{88}$$

Substituting (41) and (70) into (88) gives (89).

$$\begin{aligned}&\mathrm{P}_r\left\{\mathcal{X}^{\mathrm{III}}\middle|\left\{|h_{Is}|^2=q\right\}<\gamma_{\mathrm{th}}\right\}=1\\&-\int_0^{\infty}\frac{2\zeta_s\tau\lambda_{Ir}q}{(1-\tau)\lambda_{sr}\left(z+\gamma_{\mathrm{th}}+\frac{2\zeta_s\tau\lambda_{Ir}q}{(1-\tau)\lambda_{sr}}\right)^2}\\&\times\frac{(1-\tau)\lambda_{rd}\lambda_{Ir}}{2\zeta_r\tau\lambda_{Id}}\frac{(z+\gamma_{\mathrm{th}}+1)\gamma_{\mathrm{th}}}{z}\\&\times e^{-\left(\frac{(1-\tau)\lambda_{rd}\lambda_{Ir}}{2\zeta_r\tau\lambda_{Id}}\frac{(z+\gamma_{\mathrm{th}}+1)\gamma_{\mathrm{th}}}{z}\right)}\\&\times\mathrm{Ei}\left(-\frac{(1-\tau)\lambda_{rd}\lambda_{Ir}}{2\zeta_r\tau\lambda_{Id}}\frac{(z+\gamma_{\mathrm{th}}+1)\gamma_{\mathrm{th}}}{z}\right)\mathrm{d}z.\end{aligned}\tag{89}$$

Considering (1) (with $ab=Is$) and (89) in (84) gives $P_{\mathrm{out}}^{\mathrm{III}}$ as (90).

$$\begin{aligned}P_{\mathrm{out}}^{\mathrm{III}}&=1-\int_0^{\infty}\lambda_{Is}e^{-\lambda_{Is}q}\\&\quad\times\int_0^{\infty}\frac{2\zeta_s\tau\lambda_{Ir}q}{(1-\tau)\lambda_{sr}\left(z+\gamma_{\mathrm{th}}+\frac{2\zeta_s\tau\lambda_{Ir}q}{(1-\tau)\lambda_{sr}}\right)^2}\\&\quad\times\frac{(1-\tau)\lambda_{rd}\lambda_{Ir}}{2\zeta_r\tau\lambda_{Id}}\frac{(z+\gamma_{\mathrm{th}}+1)\gamma_{\mathrm{th}}}{z}\\&\quad\times e^{-\left(\frac{(1-\tau)\lambda_{rd}\lambda_{Ir}}{2\zeta_r\tau\lambda_{Id}}\frac{(z+\gamma_{\mathrm{th}}+1)\gamma_{\mathrm{th}}}{z}\right)}\\&\quad\mathrm{Ei}\left(-\frac{(1-\tau)\lambda_{rd}\lambda_{Ir}}{2\zeta_r\tau\lambda_{Id}}\frac{(z+\gamma_{\mathrm{th}}+1)\gamma_{\mathrm{th}}}{z}\right)\mathrm{d}z\mathrm{d}q.\end{aligned}\tag{90}$$

$$\begin{aligned}P_{\mathrm{out}}^{\mathrm{III}}&=1-\int_0^{\infty}\frac{(1-\tau)\lambda_{rd}\lambda_{Ir}}{2\zeta_r\tau\lambda_{Id}}\frac{(z+\gamma_{\mathrm{th}}+1)\gamma_{\mathrm{th}}}{z}\\&\quad\times e^{-\left(\frac{(1-\tau)\lambda_{rd}\lambda_{Ir}}{2\zeta_r\tau\lambda_{Id}}\frac{(z+\gamma_{\mathrm{th}}+1)\gamma_{\mathrm{th}}}{z}\right)}\\&\quad\times\mathrm{Ei}\left(-\frac{(1-\tau)\lambda_{rd}\lambda_{Ir}}{2\zeta_r\tau\lambda_{Id}}\frac{(z+\gamma_{\mathrm{th}}+1)\gamma_{\mathrm{th}}}{z}\right)\\&\quad\left[\underbrace{\int_0^{\infty}\lambda_{Is}e^{-\lambda_{Is}q}\frac{2\zeta_s\tau\lambda_{Ir}q}{(1-\tau)\lambda_{sr}\left(z+\gamma_{\mathrm{th}}+\frac{2\zeta_s\tau\lambda_{Ir}q}{(1-\tau)\lambda_{sr}}\right)^2}\mathrm{d}q}_{\triangleq I_4}\right]\mathrm{d}z.\end{aligned}\tag{91}$$

Swapping the last two integrals in (90) yields (91). Finally, solving for I_4 using [54, Eq. (2.3.6.9)] along with some simplifications gives (20).

APPENDIX F
THEOREM 3.6 PROOF

The conditional SIR in (87) can be upper bounded as

$$\mathcal{X}^{\mathrm{III}}\left|\left\{|h_{Is}|^2=q\right\}\right.\le\mathcal{X}_{\mathrm{up}}^{\mathrm{III}}\left|\left\{|h_{Is}|^2=q\right\}\right.=\min\left(\frac{\mathcal{X}_1}{\Psi_1},\frac{\mathcal{Y}_2}{\Phi_2}\right).\tag{92}$$

Accordingly, the lower bounded outage probability of Mode III can be obtained by

$$P_{\mathrm{out,Low}}^{\mathrm{III}}=\int_0^{\infty}f_{|h_{Is}|^2}(q)\mathrm{P}_r\left\{\mathcal{X}_{\mathrm{up}}^{\mathrm{III}}\middle|\left\{|h_{Is}|^2=q\right\}<\gamma_{\mathrm{th}}\right\}\mathrm{d}q,\tag{93}$$

where

$$\begin{aligned}&\mathrm{P}_r\left\{\mathcal{X}_{\mathrm{up}}^{\mathrm{III}}\middle|\left\{|h_{Is}|^2=q\right\}<\gamma_{\mathrm{th}}\right\}\\&=\mathrm{P}_r\left\{\min\left(\frac{\mathcal{X}_1}{\Psi_1},\frac{\mathcal{Y}_2}{\Phi_2}\right)<\gamma_{\mathrm{th}}\right\}\\&=1-\mathrm{P}_r\left\{\frac{\mathcal{X}_1}{\Psi_1}>\gamma_{\mathrm{th}}\bigcap\frac{\mathcal{Y}_2}{\Phi_2}>\gamma_{\mathrm{th}}\right\}.\end{aligned}\tag{94}$$

It is clear that $\frac{\mathcal{X}_1}{\Psi_1}=\frac{\frac{2\zeta_s\tau}{(1-\tau)}q|h_{sr}|^2}{|h_{Ir}|^2}$ and $\frac{\mathcal{Y}_2}{\Phi_2}=\frac{\frac{2\zeta_r\tau}{(1-\tau)}|h_{rd}|^2|h_{Ir}|^2}{|h_{Id}|^2}$ are dependant. Thus, conditioned on $|h_{Ir}|^2=f$, we may obtain (95) shown at the bottom of the page. Provided that

$$F_{\frac{\mathcal{X}_1}{\Psi_1}\left|\{|h_{Ir}|^2=f\}\right.}(\gamma_{\mathrm{th}})=1-e^{-\frac{\lambda_{sr}(1-\tau)}{2\zeta_s\tau q}f\gamma_{\mathrm{th}}}\tag{96}$$

and

$$F_{\frac{\mathcal{Y}_2}{\Phi_2}\left|\{|h_{Ir}|^2=f\}\right.}(\gamma_{\mathrm{th}})=\frac{\gamma_{\mathrm{th}}}{\gamma_{\mathrm{th}}+\frac{\lambda_{Id}2\zeta_r\tau}{(1-\tau)\lambda_{rd}}f}\tag{97}$$

$$\begin{aligned}\mathrm{P}_r\left\{\mathcal{X}_{\mathrm{up}}^{\mathrm{III}}\middle|\left\{|h_{Is}|^2=q\right\}<\gamma_{\mathrm{th}}\right\}&=1-\int_0^{\infty}\mathrm{P}_r\left\{\frac{\mathcal{X}_1}{\Psi_1}\middle|\left\{|h_{Ir}|^2=f\right\}>\gamma_{\mathrm{th}}\right\}\mathrm{P}_r\left\{\frac{\mathcal{Y}_2}{\Phi_2}\middle|\left\{|h_{Ir}|^2=f\right\}>\gamma_{\mathrm{th}}\right\}f_{|h_{Ir}|^2}(f)df\\&=1-\int_0^{\infty}\left[1-F_{\frac{\mathcal{X}_1}{\Psi_1}\left|\{|h_{Ir}|^2=f\}\right.}(\gamma_{\mathrm{th}})\right]\left[1-F_{\frac{\mathcal{Y}_2}{\Phi_2}\left|\{|h_{Ir}|^2=f\}\right.}(\gamma_{\mathrm{th}})\right]f_{|h_{Ir}|^2}(f)df\end{aligned}\tag{95}$$

$$\mathrm{P}_r\left\{\mathcal{X}_{\mathrm{up}}^{\mathrm{II}}\middle|\left\{|h_{Is}|^2=q\right\}<\gamma_{\mathrm{th}}\right\}=1-\frac{\Gamma(2)\lambda_{Ir}\lambda_{rd}(1-\tau)\gamma_{\mathrm{th}}}{2\zeta_r\tau\lambda_{Id}}\Psi\left(2,2;\frac{\lambda_{rd}(1-\tau)\gamma_{\mathrm{th}}}{2\zeta_r\tau\lambda_{Id}}\left(\lambda_{Ir}+\frac{\lambda_{sr}(1-\tau)\gamma_{\mathrm{th}}}{2\zeta_s\tau q}\right)\right). \tag{99}$$

$$P_{\mathrm{out,Low}}^{\mathrm{III}}=1-\lambda_{Is}\frac{\Gamma(2)\lambda_{Ir}\lambda_{rd}(1-\tau)\gamma_{\mathrm{th}}}{2\zeta_r\tau\lambda_{Id}}\int_0^{\infty}e^{-\lambda_{Is}q}\Psi\left(2,2;\frac{\lambda_{rd}(1-\tau)\gamma_{\mathrm{th}}}{2\zeta_r\tau\lambda_{Id}}\left(\lambda_{Ir}+\frac{\lambda_{sr}(1-\tau)\gamma_{\mathrm{th}}}{2\zeta_s\tau q}\right)\right)\mathrm{d}q \tag{100}$$

$$P_{\mathrm{out,Low}}^{\mathrm{III}}=1-\lambda_{Is}\frac{\Gamma(2)\lambda_{Ir}\lambda_{rd}(1-\tau)\gamma_{\mathrm{th}}}{2\zeta_r\tau\lambda_{Id}}\sum_{k=0}^{n}\frac{(-1)^k(2)_k(1)_k}{k!}\left(\frac{4\zeta_s\zeta_r\tau^2\lambda_{Id}}{\lambda_{rd}(1-\tau)^2\gamma_{\mathrm{th}}}\right)^{k+2}\int_0^{\infty}\frac{e^{-\lambda_{Is}q}q^{k+2}}{\left(\lambda_{sr}\gamma_{\mathrm{th}}+\frac{2\zeta_s\tau\lambda_{Ir}}{1-\tau}q\right)^{k+2}} \tag{101}$$

gives

$$\begin{aligned}&\mathrm{P}_r\left\{\mathcal{X}_{\mathrm{up}}^{\mathrm{II}}\middle|\left\{|h_{Is}|^2=q\right\}<\gamma_{\mathrm{th}}\right\}\\&=1-\int_0^{\infty}\lambda_{Ir}e^{-\left[\lambda_{Ir}+\frac{(1-\tau)\lambda_{sr}\gamma_{\mathrm{th}}}{2\zeta_s\tau q}\right]f}\\&\quad\times\frac{\frac{\lambda_{Id}2\zeta_r\tau}{(1-\tau)\lambda_{rd}}f}{\gamma_{\mathrm{th}}+\frac{\lambda_{Id}2\zeta_r\tau}{(1-\tau)\lambda_{rd}}f}df.\end{aligned} \tag{98}$$

With the help of [54, Eq. (2.3.6.9)] we obtain (99) shown at the top of this page. Now, substituting (99) and (1) with $ab = Is$ into (93) gives (100) shown at the top of this page. The integral in (100) has unknown closed-form solution. However, using the fact that

$$\Psi(a,b,z)\approx\frac{1}{z^a}\sum_{k=0}^{n}\frac{(-1)^k(a)_k(a-b+1)_k}{k!}\frac{1}{z^k}$$

for large z in (100) gives (101) shown at the top of this page. Solving the integral in (101) using [54, Eq. (2.3.6.9)] finally gives (22), which completes the proof.

REFERENCES

[1] C. Despins et al., "Leveraging green communications for carbon emission reductions: Techniques, testbeds, and emerging carbon footprint standards," *IEEE Commun. Mag.*, vol. 49, no. 8, pp. 101–109, Aug. 2011.

[2] F. R. Yu, X. Zhang, and V. C. Leung, *Green Communications and Networking*. Boca Raton, FL, USA: CRC Press, 2016.

[3] S. Cui, A. Goldsmith, and A. Bahai, "Energy-efficiency of MIMO and cooperative MIMO techniques in sensor networks," *IEEE J. Sel. Areas Commun.*, vol. 22, no. 6, pp. 1089–1098, Aug. 2004.

[4] N. Zhao, F. R. Yu, and H. Sun, "Adaptive energy-efficient power allocation in green interference-alignment-based wireless networks," *IEEE Trans. Veh. Technol.*, vol. 64, no. 9, pp. 4268–4281, Sep. 2015.

[5] X. Lu, P. Wang, D. Niyato, D. I. Kim, and Z. Han, "Wireless networks with RF energy harvesting: A contemporary survey," *IEEE Commun. Surveys Tuts.*, vol. 17, no. 2, pp. 757–789, Second Quarter 2015.

[6] H. J. Visser and R. J. M. Vullers, "RF energy harvesting and transport for wireless sensor network applications: Principles and requirements," *Proc. IEEE*, vol. 101, no. 6, pp. 1410–1423, Jun. 2013.

[7] S. Kim et al., "Ambient RF energy-harvesting technologies for self-sustainable standalone wireless sensor platforms," *Proc. IEEE*, vol. 102, no. 11, pp. 1649–1666, Nov. 2014.

[8] Q. Liu, M. Golinński, P. Pawełczak, and M. Warnier, "Green wireless power transfer networks," *IEEE J. Sel. Areas Commun.*, vol. 34, no. 5, pp. 1740–1756, May 2016.

[9] F. Rezaei, C. Tellambura, and S. Herath, "Large-scale wireless-powered networks with backscatter communications–A comprehensive survey," *IEEE Open J. Commun. Soc.*, vol. 1, pp. 1100–1130, 2020.

[10] X. Mou and H. Sun, "Wireless power transfer: Survey and roadmap," in *Proc. IEEE 81st Veh. Technol. Conf.*, 2015, pp. 1–5.

[11] D. Niyato, D. I. Kim, M. Maso, and Z. Han, "Wireless powered communication networks: Research directions and technological approaches," *IEEE Wireless Commun.*, vol. 24, no. 6, pp. 88–97, Dec. 2017.

[12] K. Huang, C. Zhong, and G. Zhu, "Some new research trends in wirelessly powered communications," *IEEE Wireless Commun.*, vol. 23, no. 2, pp. 19–27, Apr. 2016.

[13] T. D. P. Perera, D. N. K. Jayakody, S. K. Sharma, S. Chatzinotas, and J. Li, "Simultaneous wireless information and power transfer (SWIPT): Recent advances and future challenges," *IEEE Commun. Surveys Tuts.*, vol. 20, no. 1, pp. 264–302, First Quarter 2018.

[14] I. Krikidis, S. Timotheou, S. Nikolaou, G. Zheng, D. W. K. Ng, and R. Schober, "Simultaneous wireless information and power transfer in modern communication systems," *IEEE Commun. Mag.*, vol. 52, no. 11, pp. 104–110, Nov. 2014.

[15] L. R. Varshney, "Transporting information and energy simultaneously," in *Proc. IEEE Int. Symp. Inf. Theory*, 2008, pp. 1612–1616.

[16] S. Atapattu and J. Evans, "Optimal energy harvesting protocols for wireless relay networks," *IEEE Trans. Wireless Commun.*, vol. 15, no. 8, pp. 5789–5803, Aug. 2016.

[17] R. Tao, A. Salem, and K. A. Hamdi, "Adaptive relaying protocol for wireless power transfer and information processing," *IEEE Commun. Lett.*, vol. 20, no. 10, pp. 2027–2030, Oct. 2016.

[18] T. N. Do, D. B. da Costa, T. Q. Duong, and B. An, "Improving the performance of cell-edge users in MISO-NOMA systems using TAS and SWIPT-based cooperative transmissions," *IEEE Trans. Green Commun. Netw.*, vol. 2, no. 1, pp. 49–62, Mar. 2018.

[19] M. K. Atiq, U. Schilcher, X. Pengili, M. Haenggi, and C. Bettstetter, "Burstiness of interference pikes in wireless networks," *IEEE Open J. Veh. Technol.*, vol. 4, pp. 293–309, 2023.

[20] N. Zhao, S. Zhang, F. R. Yu, Y. Chen, A. Nallanathan, and V. C. M. Leung, "Exploiting interference for energy harvesting: A survey, research issues, and challenges," *IEEE Access*, vol. 5, pp. 10403–10421, 2017.

[21] Y. H. Al-Badarneh, C. N. Georghiades, and M.-S. Alouini, "On the throughput of interference-based wireless powered communications with receive antenna selection," *IEEE Trans. Veh. Technol.*, vol. 69, no. 3, pp. 3048–3056, Mar. 2020.

[22] J. G. Andrews et al., "What will 5G be?," *IEEE J. Sel. Areas Commun.*, vol. 32, no. 6, pp. 1065–1082, Jun. 2014.

[23] U. Uyoata, J. Mwangama, and R. Adeogun, "Relaying in the Internet of Things (IOT): A survey," *IEEE Access*, vol. 9, pp. 132675–132704, 2021.

[24] A. A. Amin and S. Y. Shin, "Capacity analysis of cooperative NOMA-OAM-MIMO based full-duplex relaying for 6G," *IEEE Wireless Commun. Lett.*, vol. 10, no. 7, pp. 1395–1399, Jul. 2021.

[25] G. Srirutchataboon and S. Sugiura, "Secrecy performance of buffer-aided hybrid virtual full-duplex and half-duplex relay activation," *IEEE Open J. Veh. Technol.*, vol. 3, pp. 344–355, 2022.

[26] J. Qiao, X. S. Shen, J. W. Mark, Q. Shen, Y. He, and L. Lei, "Enabling device-to-device communications in millimeter-wave 5G cellular networks," *IEEE Commun. Mag.*, vol. 53, no. 1, pp. 209–215, Jan. 2015.
[27] X. Ge, H. Cheng, G. Mao, Y. Yang, and S. Tu, "Vehicular communications for 5G cooperative small-cell networks," *IEEE Trans. Veh. Technol.*, vol. 65, no. 10, pp. 7882–7894, Oct. 2016.
[28] J. Zhao, X. Yue, and S. Kang, "Performance analysis of AF relaying assisted NOMA system with imperfect CSI and SIC," *Phys. Commun.*, vol. 43, 2020, Art. no. 101197.
[29] J. Zan, G. Lu, and Y. Ye, "Outage performance of UAV-assisted AF relaying with hardware impairments," *Phys. Commun.*, vol. 46, 2021, Art. no. 101334.
[30] C. Wang et al., "Cellular architecture and key technologies for 5G wireless communication networks," *IEEE Commun. Mag.*, vol. 52, no. 2, pp. 122–130, Feb. 2014.
[31] A. Gupta and R. K. Jha, "A survey of 5G network: Architecture and emerging technologies," *IEEE Access*, vol. 3, pp. 1206–1232, 2015.
[32] Y. M. Khattabi, "New analytical approach in the SER evaluation of CSIN-assisted AF dual-hop wireless systems," *IEEE Wireless Commun. Lett.*, vol. 8, no. 2, pp. 604–607, Apr. 2019.
[33] E. U. T. R. Access, "Further advancements for E-UTRA physical layer aspects," 3GPP, Sophia Antipolis, France, Tech. Specification, 2010.
[34] Y. Yang, H. Hu, J. Xu, and G. Mao, "Relay technologies for WiMAX and LTE-advanced mobile systems," *IEEE Commun. Mag.*, vol. 47, no. 10, pp. 100–105, Oct. 2009.
[35] J. N. Laneman and G. W. Wornell, "Distributed space-time-coded protocols for exploiting cooperative diversity in wireless networks," *IEEE Trans. Inf. Theory*, vol. 49, no. 10, pp. 2415–2425, Oct. 2003.
[36] J. N. Laneman, D. N. C. Tse, and G. W. Wornell, "Cooperative diversity in wireless networks: Efficient protocols and outage behavior," *IEEE Trans. Inf. Theory*, vol. 50, no. 12, pp. 3062–3080, Dec. 2004.
[37] A. Sendonaris, E. Erkip, and B. Aazhang, "User cooperation diversity. Part I. System description," *IEEE Trans. Commun.*, vol. 51, no. 11, pp. 1927–1938, Nov. 2003.
[38] A. Sendonaris, E. Erkip, and B. Aazhang, "User cooperation diversity. Part II. Implementation aspects and performance analysis," *IEEE Trans. Commun.*, vol. 51, no. 11, pp. 1939–1948, Nov. 2003.
[39] Y. M. Khattabi, "CSIN-assisted AF dual-hop relaying communication systems over imperfect Nagakami-m fading channels: Exact error performance," *Phys. Commun.*, vol. 53, 2022, Art. no. 101717. [Online]. Available: https://www.sciencedirect.com/science/article/pii/S1874490722000659
[40] A. A. Nasir, X. Zhou, S. Durrani, and R. A. Kennedy, "Relaying protocols for wireless energy harvesting and information processing," *IEEE Trans. Wireless Commun.*, vol. 12, no. 7, pp. 3622–3636, Jul. 2013.
[41] M. Ju, K. Kang, K. Hwang, and C. Jeong, "Maximum transmission rate of PSR/TSR protocols in wireless energy harvesting DF-based relay networks," *IEEE J. Sel. Areas Commun.*, vol. 33, no. 12, pp. 2701–2717, Dec. 2015.
[42] A. Subhash and S. Kalyani, "Cooperative relaying in a SWIPT network: Asymptotic analysis using extreme value theory for non-identically distributed RVs," *IEEE Trans. Commun.*, vol. 69, no. 7, pp. 4360–4372, Jul. 2021.
[43] T. M. Hoang, B. C. Nguyen, P. T. Tran, and L. T. Dung, "Outage analysis of RF energy harvesting cooperative communication systems over Nakagami-*m* fading channels with integer and non-integer *m*," *IEEE Trans. Veh. Technol.*, vol. 69, no. 3, pp. 2785–2801, Mar. 2020.
[44] E. Illi, F. E. Bouanani, and F. Ayoub, "On the performance of dual-hop SWIPT-based relaying system with asymmetric fading conditions," in *Proc. 3rd Int. Conf. Adv. Commun. Technol. Netw.*, 2020, pp. 1–7.
[45] M. Babaei, Ü. Aygölü, and E. Basar, "Cooperative AF relaying with energy harvesting in Nakagami-m fading channel," *Phys. Commun.*, vol. 34, pp. 105–113, 2019.
[46] Y. Gu and S. Aïssa, "RF-based energy harvesting in decode-and-forward relaying systems: Ergodic and outage capacities," *IEEE Trans. Wireless Commun.*, vol. 14, no. 11, pp. 6425–6434, Nov. 2015.
[47] Y. Chen, "Energy-harvesting AF relaying in the presence of interference and Nakagami-*m* fading," *IEEE Trans. Wireless Commun.*, vol. 15, no. 2, pp. 1008–1017, Feb. 2016.
[48] Z. Liu, P. Wu, D. B. da Costa, and M. Xia, "Cooperative relaying with energy harvesting: Performance analysis using extreme value theory," in *Proc. IEEE 89th Veh. Technol. Conf.*, 2019, pp. 1–6.
[49] E. Chen, M. Xia, D. B. da Costa, and S. Aïssa, "Multi-hop cooperative relaying with energy harvesting from cochannel interferences," *IEEE Commun. Lett.*, vol. 21, no. 5, pp. 1199–1202, May 2017.
[50] S. S. Kalamkar and A. Banerjee, "Interference-aided energy harvesting: Cognitive relaying with multiple primary transceivers," *IEEE Trans. Cogn. Commun. Netw.*, vol. 3, no. 3, pp. 313–327, Sep. 2017.
[51] N. Deng and M. Haenggi, "The energized point process as a model for wirelessly powered communication networks," *IEEE Trans. Green Commun. Netw.*, vol. 4, no. 3, pp. 832–844, Sep. 2020.
[52] I. Gradshteyn and I. Ryzhik, "Table of integrals, series and products 5th edn ed a jeffrey and D," in *Zwillinger*. New York, NY, USA: Academic, 2007.
[53] M. Hanif, H.-C. Yang, and M.-S. Alouini, "Receive antenna selection for underlay cognitive radio with instantaneous interference constraint," *IEEE Signal Process. Lett.*, vol. 22, no. 6, pp. 738–742, Aug. 2015.
[54] I. U. A. B. A. P. Prudnikov and O. I. Marichev, *Integrals and Series. 1 Elementary Functions*, New York, NY, USA: Taylor Francis, 2002.

YAZID M. KHATTABI (Member, IEEE) received the Ph.D. degree in electrical engineering with a specialization in wireless communications from the Center for Wireless Communications, University of Mississippi, Oxford, MS, USA, in 2016. Then, he joined the Department of Electrical Engineering, University of Jordan, Amman, Jordan, as Assistant Professor and in 2020, he promoted to the rank of Associate Professor. In 2023, he joined the College of Engineering and Technology, American University of the Middle East, Egaila, Kuwait, as an Associate Professor. From 2011 to 2012, he was a Telecommunications and Electronics Design Engineer with King Abdullah II Design and Development Bureau, Amman, Jordan. His research interests include the applications of wireless communication and information theories to the modeling and performance study of cutting-edge wireless communication technologies including and not limited to reconfigurable intelligent surfaces communications, relaying and cooperative communications, cognitive radio based communications, MIMO and spatial modulation communications, high-speed-railway communications, wireless powered communications, Internet of Things communications, lightweight encryption algorithms, vehicular and unmanned-aerial-vehicle communications, and Tera-Hz communications. He is also a Reviewer of several refereed international journals and conferences.

YAZAN H. AL-BADARNEH (Member, IEEE) born in Irbid, Jordan, in 1987. He received the Ph.D. degree in electrical engineering from Texas A & M University, College Station, TX, USA, in 2018. Following his graduation, he joined the Department of Electrical Engineering, The University of Jordan, Amman, Jordan, as an Assistant Professor. In 2023, in recognition of his academic contributions, he was promoted to the rank of Associate Professor with the Department of Electrical Engineering. His scholarly pursuits predominantly focus on the application of information and communication theories to contemporary wireless communication systems, placing particular emphasis on modeling, design, and performance analysis.

MOHAMED-SLIM ALOUINI (Fellow, IEEE) was born in Tunis, Tunisia. He received the Ph.D. degree in electrical engineering from the California Institute of Technology, Pasadena, CA, USA, in 1998. He was a Faculty Member with the University of Minnesota, Minneapolis, MN, USA, Texas A & M University at Qatar, Ar-Rayyan, Qatar, before joining in 2009 the King Abdullah University of Science and Technology (KAUST), Thuwal, Saudi Arabia, where he is currently the Al-Khawarizmi Distinguished Professor of electrical and computer engineering. Dr. Alouini is a Fellow of the OPTICA (Formerly the Optical Society of America (OSA)). He is currently particularly interested in addressing the technical challenges associated with the uneven distribution, access to, and use of information and communication technologies in rural, low-income, disaster, and/or hard-to-reach areas.